Progress Report and Renewal Request for R&D on

Precision Straw Tube Tracking

(Submitted to the Superconducting Super Collider Laboratory)

W.S. Anderson, J.C. Armitage,[1] E. Dunn, J.G. Heinrich, C. Lu, K.T. McDonald,[2]
J. Weckel, and Y. Zhu

Joseph Henry Laboratories, Princeton University, Princeton, NJ 08544

(September 15, 1991)

Summary

We present a brief summary of work accomplished at Princeton U. in FY91 towards a straw-tube tracking subsystem with precision spatial resolution at the SSC. A budget of **$213k** is proposed for FY92 to continue this work. Of these funds about 1/3 are for continued characterization of single-electron avalanches, including measurement of drift velocity, the first Townsend coefficient, the attachment coefficient, and the gas gain. The remaining funds are for a second phase of construction of a prototype straw-tube system, with emphasis on coaxial construction of the mechanical and electrical connection between the straw-tube electrodes and the front-end electronics.

[1] on sabbatical from Carleton U.

[2] Contactperson

Contents

List of Figures

1 Progress Report

1.1 Overview

The R&D on straw-tube tracking conducted at Princeton over the past two years has been motivated by its potential application to a B-physics experiment. This leads us to set goals that may be somewhat different from those of groups motivated by experiments for the Higgs sector. We take as our goals:

- A tracking system of moderate cost that complements an inner silicon vertex detector by providing precision momentum measurement in a magnetic field.
- Spatial resolution of 50 μm is desired.
- The system need operate only at luminosities of 10^{32} cm^{-2}sec^{-1} or less. This permits slower drift velocities, as may be useful to achieve finer spatial resolution. Also, radiation damage will be less severe, and the system can extend to with 10-15 cm of the beams.
- The maximum straw-tube length is about 2 m, in keeping with the relatively compact configuration of a B-physics experiment.
- As the channel count of a straw-tube system in a B-physics experiment amy well exceed 10^5, the readout electronics should be inexpensive, low power, and capable of digital buffering near the detector to minimize the cable plant.

To realize these goals we have initiated a program of study to provide detailed characterization of the chamber signals, and also to demonstrate overall system performance via prototype straw-tube modules.

Work performed in previous fiscal years has been reported elsewhere [1, 2, 3, 4, 5, 6], and three preliminary reports [7, 8, 9] describe work in FY91.

1.2 Characterization of Single-Electron Avalanches

Gas proportional counters, such as straw-tube chambers, can be used as position-sensitive detectors by measurement of the time of flight to the anode wire of electrons ionized by a passing charged particle. Some 30-100 electrons are liberated per cm of path length, so the time of arrival of the first of the electrons is a good measure of the impact parameter of the passing particle [10], so long as this is greater than the mean distance between ionizations, *i.e.*, 100-300 μm. A detailed understanding of the performance of such a detector depends on knowledge of the statistics of the primary ionization and of the gas-gain mechanism, as well as of the field-dependent drift velocity of electrons in the chamber gas.

We have developed a technique to study single photoelectrons ejected from the wall of a proportional tube chamber by a N_2 laser. Measurements of avalanche size and of drift time have been made thereby, without the usual uncertainty as to the amount of primary ionization. Of course, a complete survey of the relevant properties of chamber gases must include measurement of the primary-ionization density, but we have deferred this for the time being.

1.2.1 Experimental Set-Up

A sketch of the experimental set-up is shown in Fig. 1. Figure 2 gives details of a test chamber that permits both a laser beam and an Fe^{55} source to be used to generate the primary electrons.

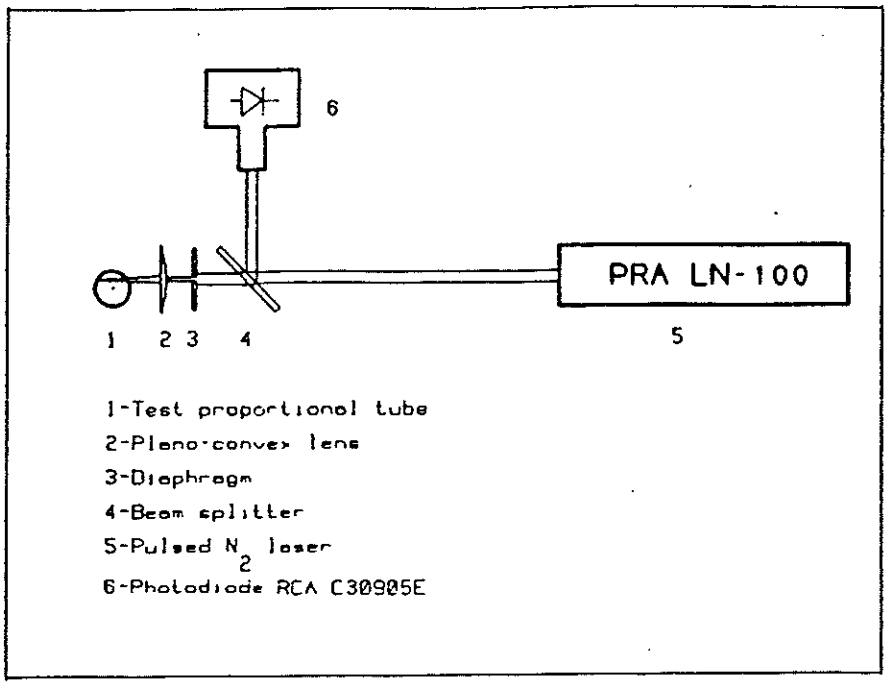

Figure 1: Sketch of the experimental set-up for studies of single-photoelectron avalanches.

The N_2 laser generates pulsed 337-nm (3.67-eV) UV photons, with a pulse length of about 350 ps. The pulse energy is about 50 μJ, corresponding to about 10^{14} photons. The first test drift tube was made of 7.67-mm-diameter aluminum tubing. Later three different size of test drift tubes were installed into this chamber with diameters of 3.3, 4.83, and 6.1 mm, respectively.

The photoelectric work function of aluminum is 4.08 eV, which is larger than laser-beam energy; therefore the quantum efficiency for producing the photoelectron from the wall is expected to be very small. Still, the work function of aluminum is smaller than that of copper or stainless steel, so it is favorable to work with the former material. But due to the large number of photons per pulse we still can get more than enough photoelectrons. As we are most interested in single-photoelectron events, we use an iris diaphragm to reduce the beam intensity.

The laser beam was focused onto the inner wall of the aluminum tube after passing through a 1-mm-diameter hole in the wall. A beam splitter upstream was used to reflect part of the laser beam to an avalanche photodiode (RCA C30905E), which generates a trigger pulse. An EG&G ORTEC 142PC charge-sensitive preamplifier was directly connected to the

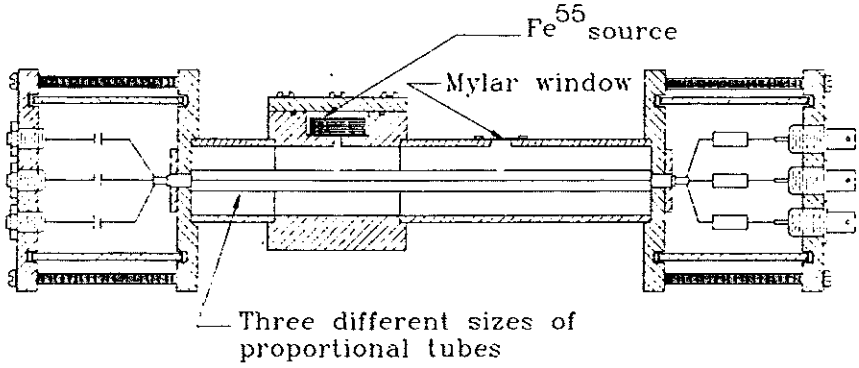

Figure 2: Details of the test chamber.

test drift tube through a high-voltage capacitor. The preamp was followed by an Ortec model 570 spectroscopy amplifier, whose output was digitized by an Ortec model 916 multichannel analyzer. A calibration of the charge out of the chamber per count in the 916 analyzer was obtained with an Ortec model 419 precision pulser (by charging a 2 pf capacitor). Figure 3 shows a block diagram of the electronics.

To blend different gas mixtures and to adjust the gas pressure with high precision, a bench-top gas system was installed, as shown in Fig. 4.

The accuracy of the mass-flow controllers is 2% of reading and the accuracy of pressure transducer is 0.15% of reading (according to the manufacturers' specifications, Vacuum General, and Edwards High Vacuum, respectively). The fluctuation of the pressure under control has been within ± 1 torr around the set point.

The piping of whole system was made of copper tubing. An oxygen filter and a moisture filter were installed directly in front of the test prototype. According to the manufacturer's specification (Chrompak) the Gas-Clean oxygen filter removes oxygen, traces of sulphur and chlorine compounds from the gas, and the moisture filter removes water, oil, and other foreign material.

1.2.2 Gas-Gain Studies

For each gas mixture we first adjusted the iris diaphragm until only one in 10-20 laser pulses yielded any photoelectrons. This insured that we had only a single photoelectron in 90-95

The single-electron-avalanche spectra in Ar/isobutane, Ar/C_2H_6, P-10, Ar/CO_2, $Ar/CF_4/C_2H_2$ and CF_4/isobutane/C_2H_2 have been measured for several different mixing ratios. The single-electron-avalanche spectra were then fitted with the Polya distribution [11].

$$P(a) \propto (ba/\bar{a})^{b-1} e^{-ba/\bar{a}},$$

where a is the amplitude of an avalanche, $\bar{a}$ is the mean gas gain, and b is a measure of the fluctuation of gas gain: $(\sigma_a/a)^2 = 1/b$. Typical experimental distributions with their Polya

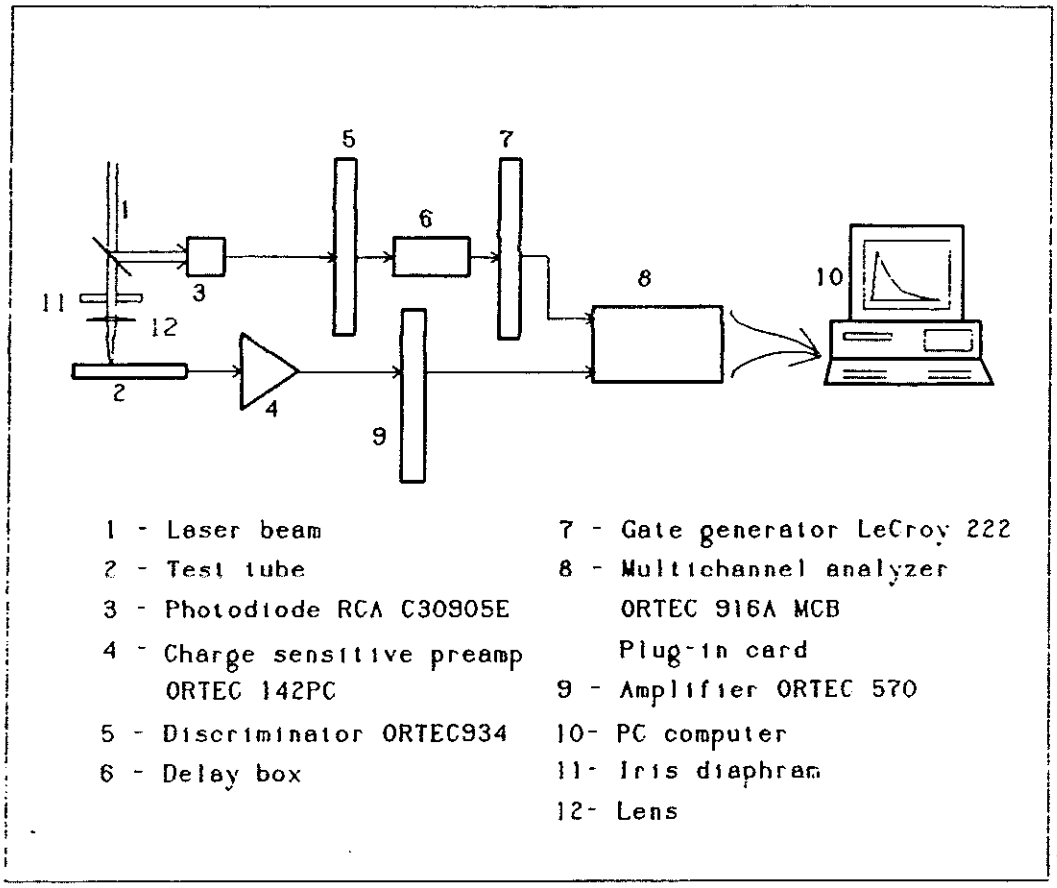

Figure 3: Electronics for single-electron-avalanche measurements.

fitting curves are shown in Fig. 5a, and the mean gas gain a is plotted *vs.* chamber voltage in Fig. 5b.

It is typical of many gas mixtures that the pulse-height (gain) spectrum of single-electron avalanches does not show a peak for mean gains of less than 10^5. This is of some significance for the operation of cylindrical proportional counters as drift chambers, where good spatial resolution requires sensitivity to the first ionization electron. At low gas gains the electronic threshold must be very much less than the mean gain to maintain high efficiency. Furthermore, the large spread in pulse height will aggravate slewing in the timing measurements.

Thus it appears that for precision timing measurements even if an electronic threshold can be set at a gas gain of 10^4, one should operate the chamber with a mean gain of about 10^5. For applications where lesser spatial resolution is required, the chamber can be run with a mean gain closer to the electronic threshold, with a consequent inefficiency on the detection of individual electron avalanches.

We also studied the avalanches caused by the 5.9-keV x-ray from an Fe^{55} source, which provides a primary ionization of about 200 electrons. For gas gains larger than 2.5×10^4, the

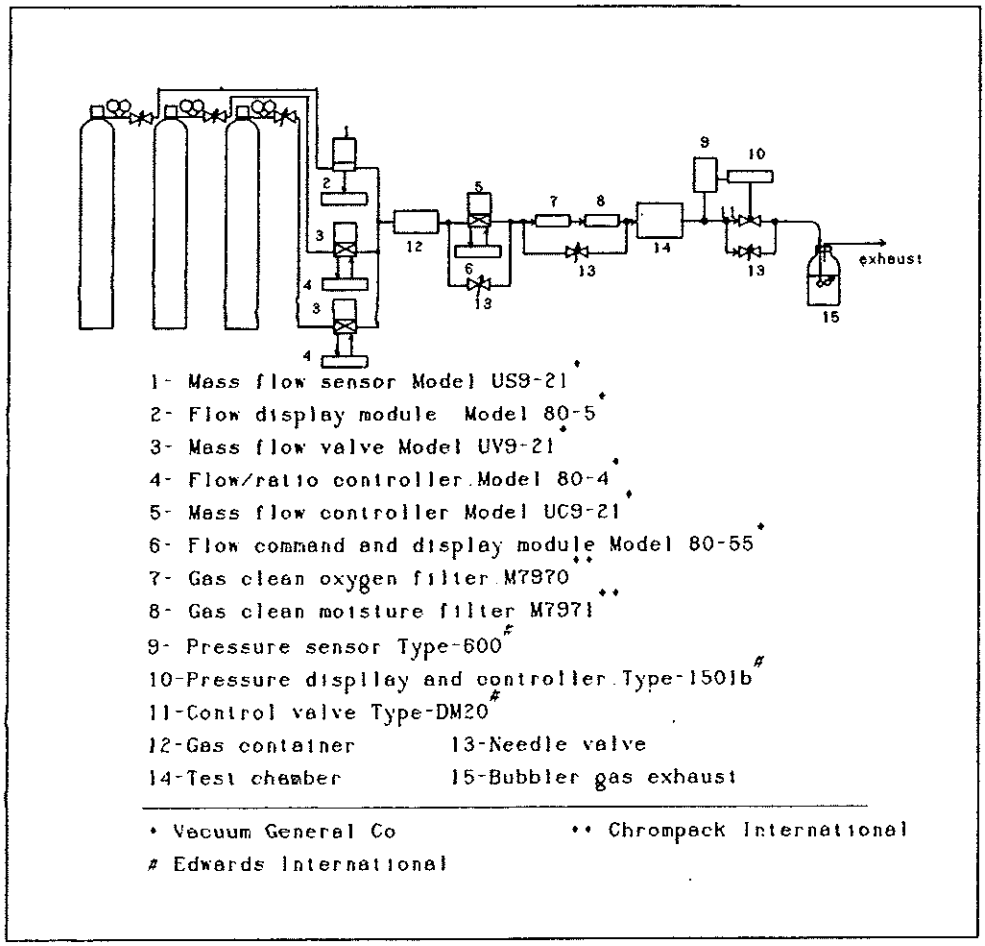

Figure 4: The gas control system.

signal charge due to the 5.9-keV x-rays will exceed 1 pC and the chamber will no longer be in the proportional mode. Therefore we have restricted our studies with Fe^{55} to gains below this value. Figure 5b shows that for Ar/Isobutane mixtures the gas gains observed with single photoelectrons, and with the Fe^{55} source agree well, taking into account the primary ionization of 200 electrons in the case of Fe^{55}.

1.2.3 Timing Studies with Single Photoelectrons

For timing studies the previous apparatus was modified by the replacement of the ORTEC preamp by a LeCroy TRA402 or a U. Penn-AT&T preamp [12], which have rise times of a few nanoseconds. Figure 6 shows the electronic block diagram.

Several conventional gas mixtures have been tested with this set-up to verify this technique. Because the laser beam spot on the inner surface of the tube is quite small, we can neglect mechanical imperfections and consider that the drift distance of the photoelectrons was just the radius of the tube R_c minus the radius of the anode wire R_a. Typical measured time spectra along with Gaussian fits for $Ar/C_2H_6(50/50)$ and $Ar/CO_2(50/50)$ are shown

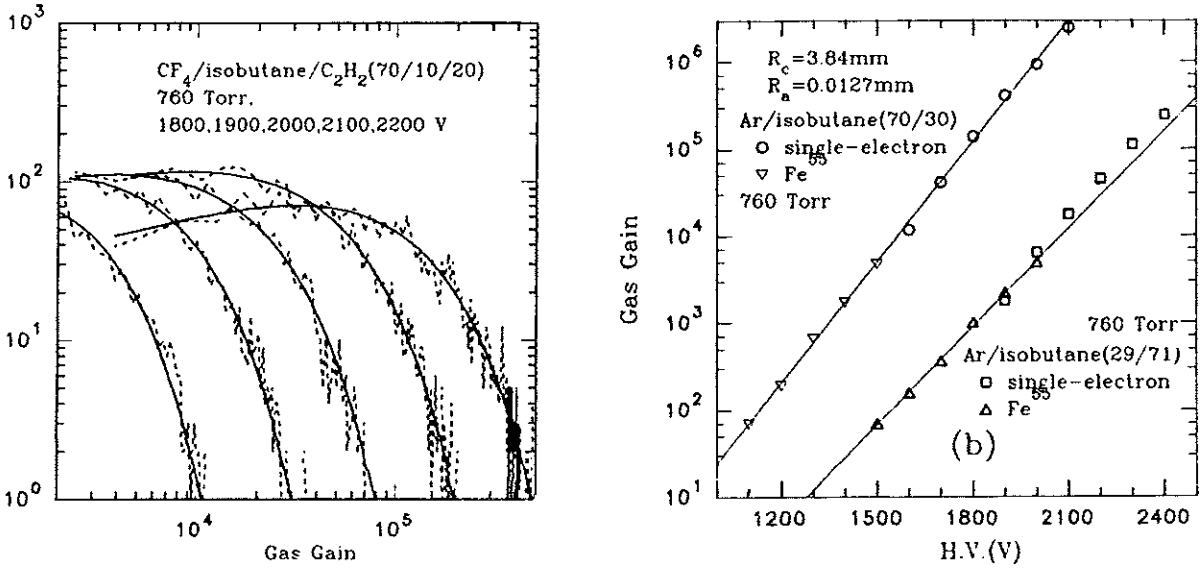

Figure 5: a) Single-electron-avalanche distributions with their Polya fittings for CF_4/isobutane/C_2H_2(70/10/20). b) Mean gas gain *vs.* chamber voltage for Ar/Isobutane mixtures.

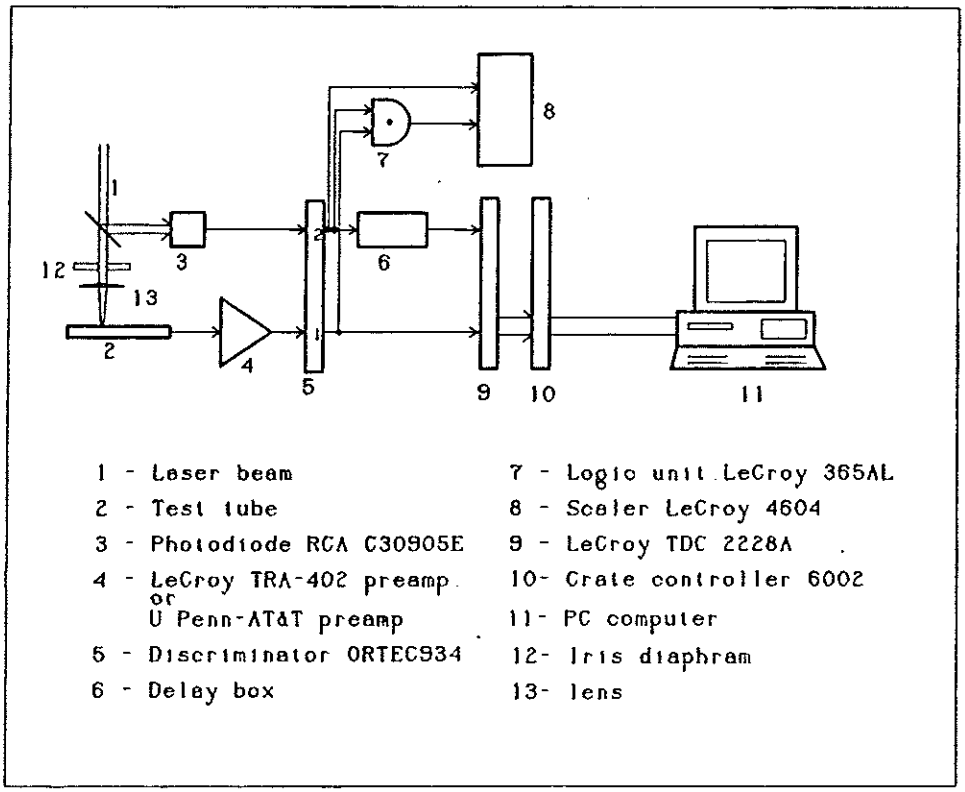

Figure 6: Block diagram of the electronics for timing studies with single photoelectrons.

in Fig. 7. The observed time resolutions of 1.9, and 2.7 ns, respectively are larger than the intrinsic resolution of our electronics, and reflect the effect of longitudinal diffusion in the chamber gas over the 3.8-mm drift path.

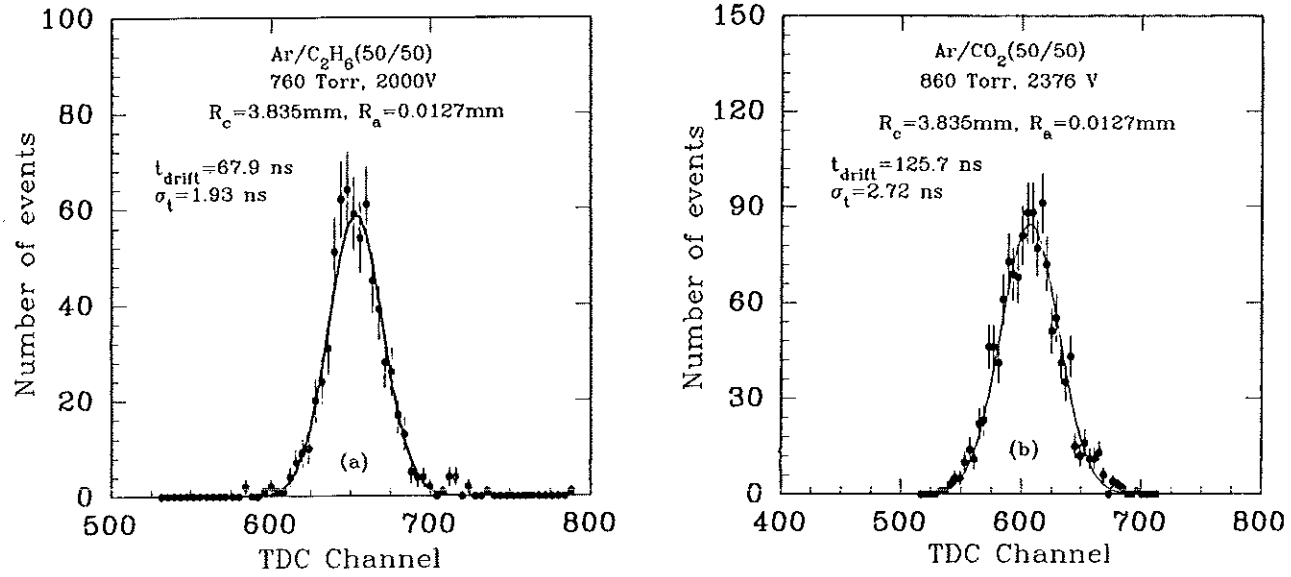

Figure 7: Drift-time spectrum for $Ar/C_2H_6(50/50)$ and $Ar/CO_2(50/50)$.

1.2.4 Spatial Resolution

To convert the observed spread in drift times into the corresponding spatial resolution we need to know the electron drift velocity as a function of field strength. We have not measured the drift velocity ourselves at this time, but propose to due so in FY92 as described in Sec. 1.2.11 below. In the meanwhile we use a model of the drift velocity.

From the kinetic theory of gases ones expects that the drift velocity should scale with E/P, where E is the electric field and P is the gas pressure. This scaling is observed to hold in the ranges of E and P relevant to proportional counters. The theory further indicates that if the mean free path and the fractional energy loss per collision are independent of the electron energy then the drift velocity should vary as $\sqrt{E/P}$. In practice, measured electron drift velocities do not always behave as $\sqrt{E/P}$, so we use simple empirical formulae to approximate the published curves on the drift velocity *vs.* E/P. From these we are able to calculate the total drift time. Adjusting the parameters in the simplified formulae to get the best fit of our data taken at various E and P, the results are shown in Fig. 8. The agreement is impressive. Because our data were collected at various pressures, and the drift velocity curves used in our fitting were measured or calculated at 1 atm, our results further confirm that drift velocity $\propto f(E/P)$.

With our technique we only measure the drift time over a distance equal to the radius of the straw tube. We have taken some data with several different straw-tube radii to further confirm our understanding of the drift velocity *vs.* E/P. From the fits to the drift velocity

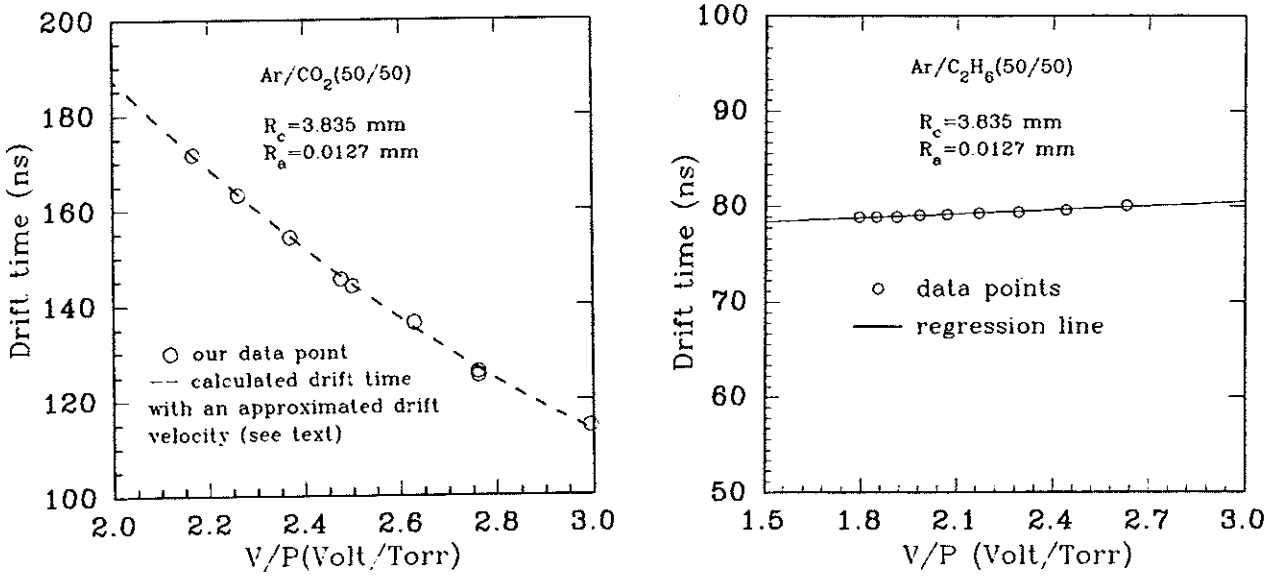

Figure 8: (a) Drift time in Ar/CO_2 (50/50). (b) Drift time in Ar/C_2H_6 (50/50).

we can then calculate the time-to-distance relation for electron motion in the straw tube. In some cases measurements of the time-to-distance relation are available for comparison. One such is shown in Fig. 9 for Ar/CO_2 ($\sim$ 50/50) where $x \propto \sqrt{t}$ at small x.

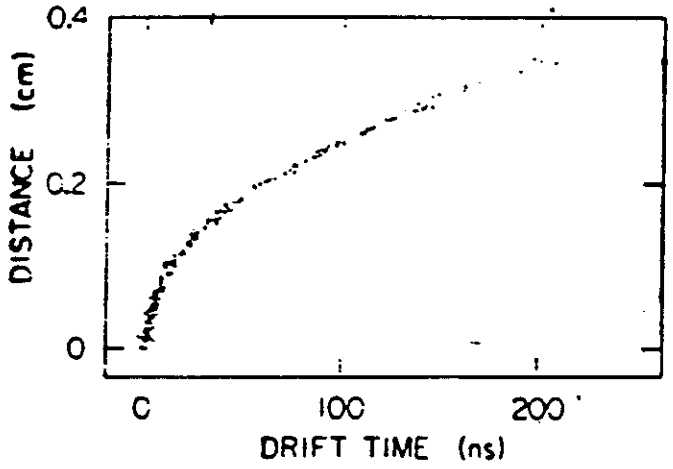

Figure 9: Time-to-distance relationship in $Ar/CO_2/CH_4$ (49.5/49.5/1.0) as measured in a straw-tube drift chamber [13].

We have measured the resolution σ_t in the drift time and convert this to the spatial

resolution σ_x using the time-to-distance relation. In general one expects

$$\sigma_t = \sqrt{2D(\epsilon)t} \approx \sqrt{2D_0 t/P},$$

as the diffusion "constant" D depends inversely on the gas density and hence pressure. Also, D is nearly independent of electron energy ϵ in many interesting cases, particularly "cool" gases such as CO_2. Then for any fixed drift distance we expect

$$\sigma_x \propto \sqrt{\frac{1}{P}}.$$

Figure 10 shows our data for σ_x as well as a fit of the form

$$\sigma_x = \sigma_0 + A/\sqrt{P}$$

for Ar/CO_2, Ar/CH_4 and Ar/C_2H_6. The addition of a (small) constant term σ_0 to the fit appears adequate to characterize the deviation of σ_x from a pure dependence on $\sqrt{1/P}$. In principle the coefficient A should vary as $\sqrt{t}$ if the drift distances varies.

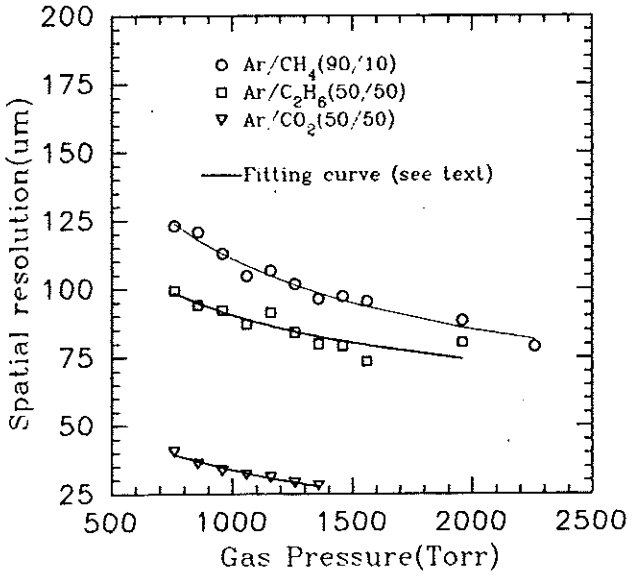

Figure 10: Spatial resolution of Ar/CH_4, Ar/C_2H_6 and Ar/CO_2 (50/50).

The total drift times over the radius of our proportional tube agree well with the published data. Direct comparison with the published data of our results on spatial resolution are difficult due to very limited existing data.

Pius [14], and also Jean-Marie *et al.* [15] have measured the longitudinal diffusion of electrons in $Ar/C_2H_6(50/50)$. We infer that $\sigma_{0l} \simeq 210\ \mu m/\sqrt{cm}$ from Pius and $\sigma_{0l} \simeq 125\ \mu m/\sqrt{cm}$ from Jean-Marie *et al.* Then for a 0.3835-cm drift distance the spatial resolutions

should be 130 μm and 77 μm, respectively. Our result for 760 torr is 100 μm, in reasonable agreement.

The spatial resolution with Ar/CO_2 (50/50) is much better than with the other two gases due to its very slow drift velocity near the tube's wall, as well as its being a "cool gas". This will not necessarily be true for signals originating close to the anode wire, noting that $x \propto \sqrt{t}$ (x distance from anode wire, t drift time), as shown in Fig. 9.

1.2.5 Timing Performance of Gas Mixtures Containing CF_4

Being convinced in the merits of our technique by the good agreement between our measurements and published data for the three gas mixtures mentioned above, we made a further investigation for gas mixtures containing CF_4.

The "fast" gas CF_4 is believed to be one of the most attractive candidates for the SSC environment [16, 17]. Recent studies [18] have demonstrated a remarkable etching property of CF_4/isobutane, which can be used for removing the wire coating caused by the gas avalanches in Ar/Ethane. CF_4 also shows excellent aging performance [19, 20, 21].

We have performed detailed experimental investigations on the timing performance for gas mixtures containing CF_4 using our single-photoelectron technique. In these U. Penn-AT&T preamplifier [12] has been employed as the superior noise performance at high frequency of this amplifier allows us to benefit from the very narrow time distribution obtainable with CF_4 gas mixtures.

Typical measured time spectra are shown in Fig. 11. We summarize the drift-time results in Fig. 12 where we see that the drift velocity for CF_4/isobutane is very sensitive to the mixing ratio, but that for Ar/CF_4 the drift velocity is much less sensitive to the mixing ratio.

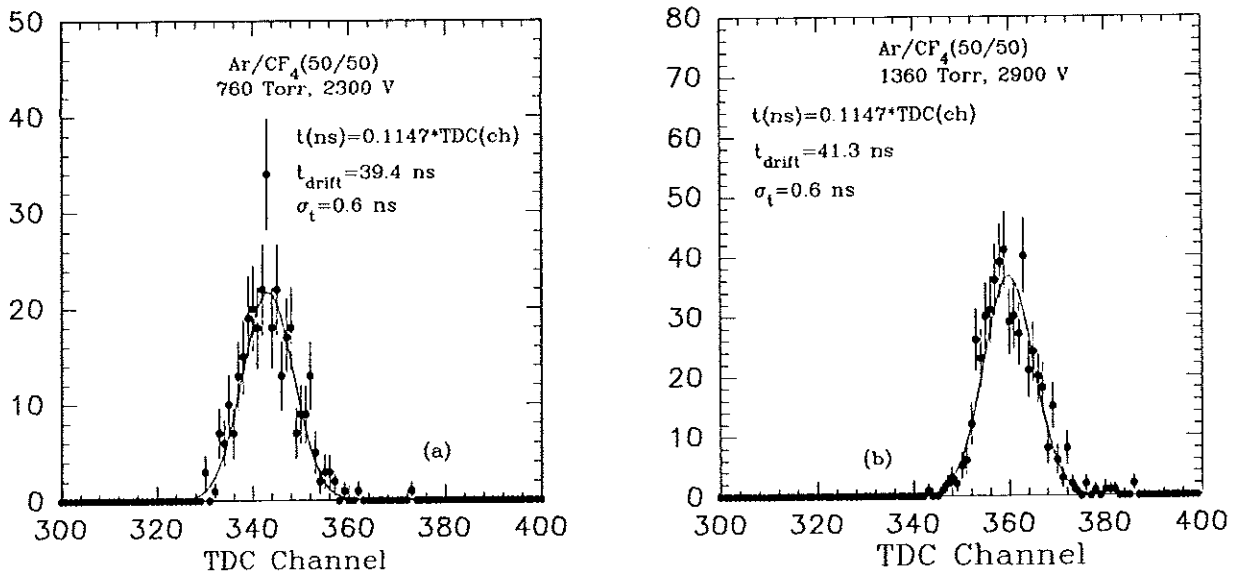

Figure 11: Typical drift time spectra of CF_4/Ar(50/50).

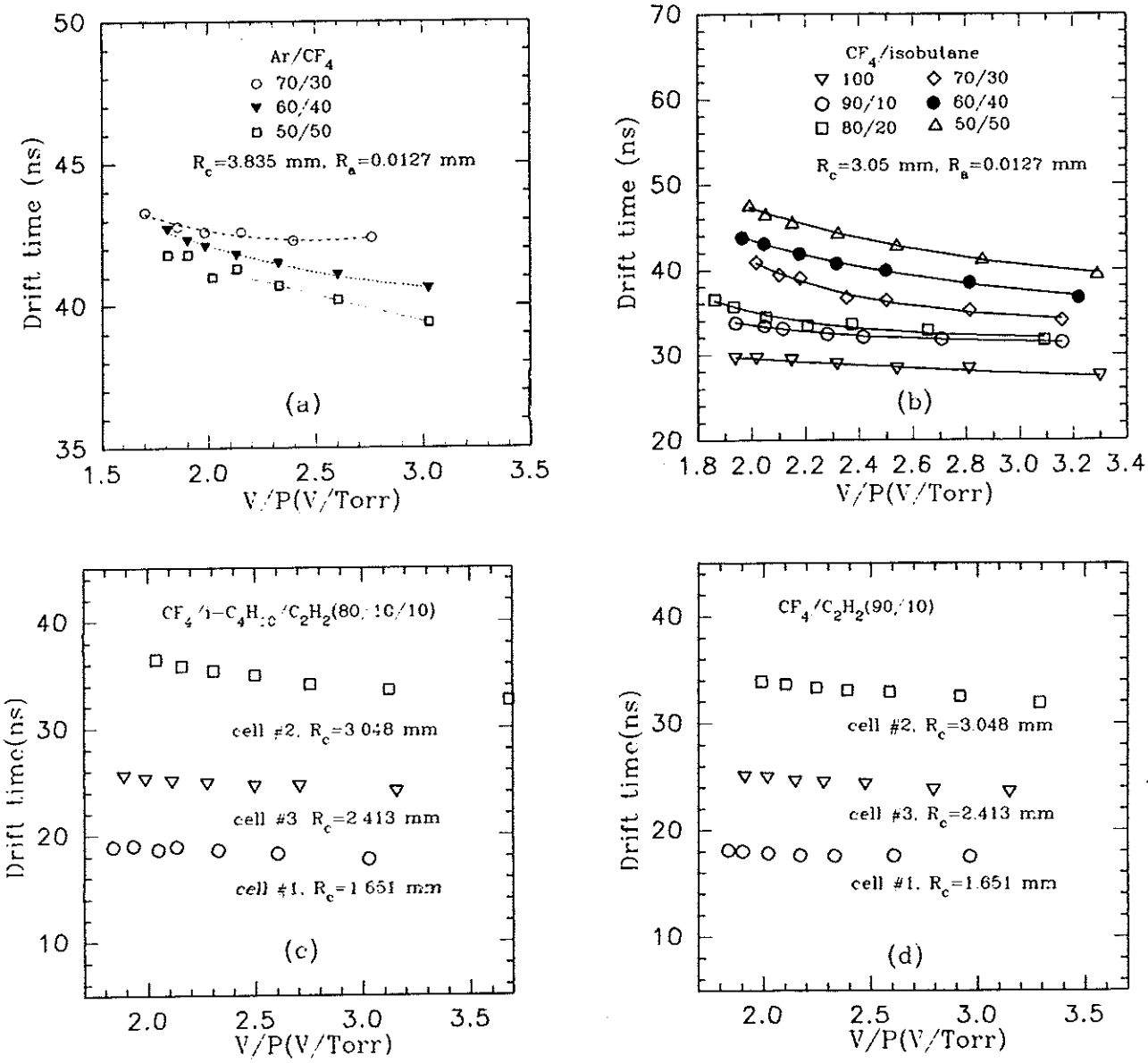

Figure 12: Total drift time of gas mixtures containing CF_4. **(a)** Ar/CF_4, **(b)** CF_4/isobutane, **(c)** CF_4/isobutane/C_2H_2 (80/10/10), **(d)** CF_4/C_2H_2(90/10).

Figure 13 shows the observed time resolution in CF_4 gas mixtures. There is little evidence that $\sigma_t \propto \sqrt{1/P}$ for these mixtures. The time resolutions are in the range 0.55-0.75 ns for Ar/CF_4 mixtures, and 0.55-1.0 ns for CF_4/isobutane mixtures. The best time resolution obtained among these mixtures is $\sim$ 0.4 ns for CF_4/C_2H_2(90/10). Because the total drift time for the latter mixture is almost constant within our measured V/P range, we can roughly estimate the position resolution from time resolution, assuming the drift velocity is

constant in a drift tube. It turns out to be ~ 32 μm. This gas also shows fast and saturated drift velocity (see Fig. 12). For $R_c = 1.651$ mm the drift time is only ~ 18 ns.

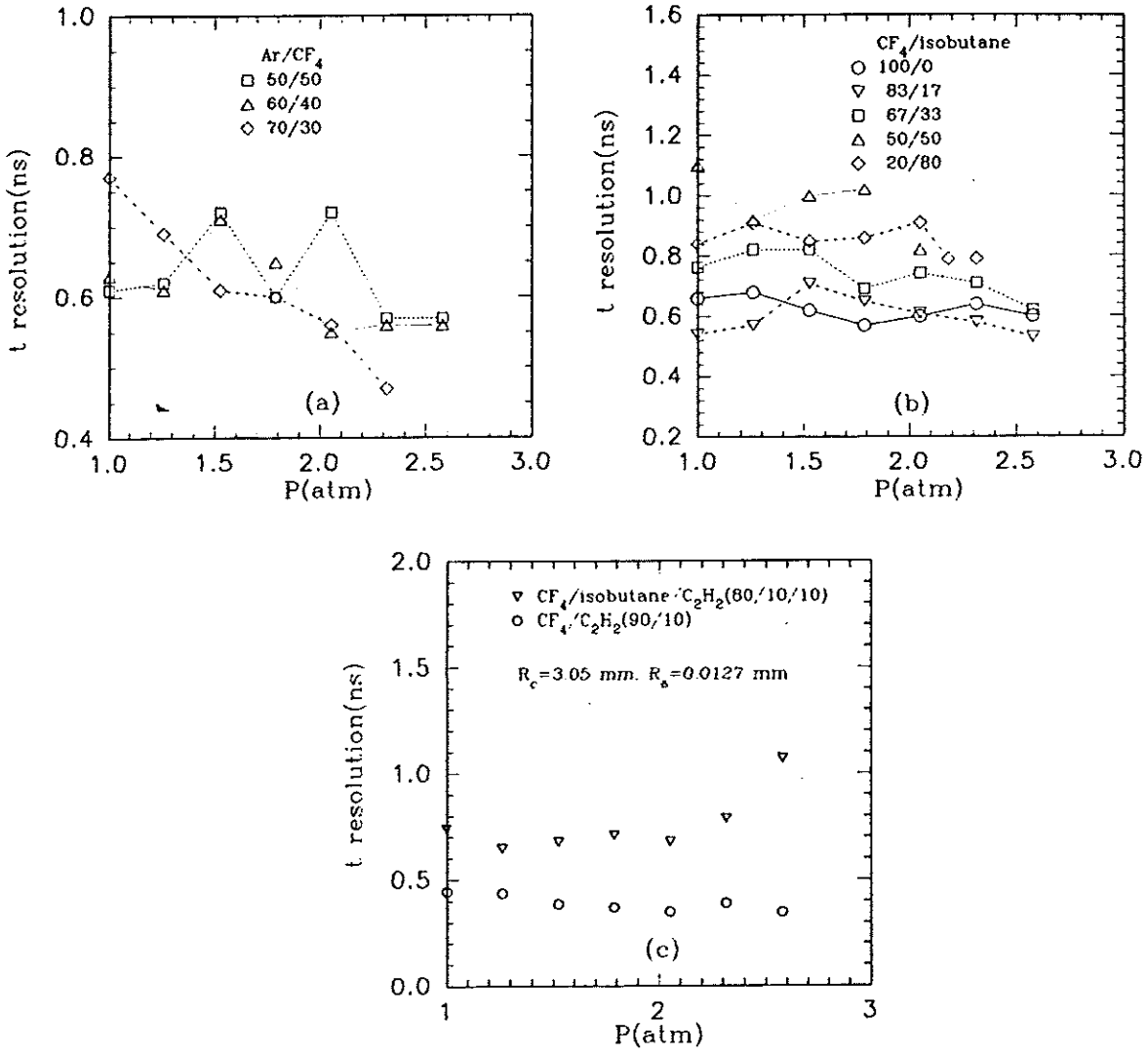

Figure 13: Drift-time resolution of gas mixtures containing CF_4. **(a)** CF_4/Ar, **(b)** CF_4/isobutane, **(c)** CF_4/isobutane/C_2H_2(80/10/10) and CF_4/C_2H_2(90/10).

1.2.6 Electron Attachment in Gas Mixtures Containing CF_4

While CF_4 gas mixtures are very advantageous from the point of view of aging, drift time, and spatial resolution, they are known [16, 17] to suffer from considerable electron attachment. This attachment can cause serious inefficiencies in the collection of electrons liberated near the anode wire, and causes broadening of the pulse-height (gain) spectrum for all ionization electrons.

In our investigations three different experimental results confirm the existence of electron attachment in the gas mixtures containing CF_4:

1. Gas gain difference between single-electron avalanches and those from Fe^{55} x-rays .

2. Degradation of energy resolution for Fe^{55} x-rays.

3. Pressure dependance of the detection efficiency for single photoelectrons.

Careful selection of the mixing ratio of the second or the third gas component can reduce this problem.

The experimental set-up was that shown in Figs. 1-4 above.

The first type of evidence of presence of electron attachment in the chamber gas was obtained as follows. Pulse-height (gain) spectra were recorded for each gas mixture at several different high voltages using an Fe^{55} source as well as single photoelectrons from the N_2 laser. If the signal size observed with the Fe^{55} source is not $\sim$ 200 times that from a single photoelectron ejected by a laser pulse, then attachment has occurred. Comparisons of avalanches due to single photoelectrons with those from Fe^{55} x-rays are shown in Fig. 14.

The conventional drift chamber gas mixtures, such as Ar/C_2H_6, Ar/CO_2, P-10 and Ar/isobutane gave rather consistent results, both from single electrons as well as from Fe^{55} x-rays. This convinced us that the gas system had little contamination and the technique for single-electron-avalanche measurement was reliable.

Then when CF_4 gas mixtures were tested, the large discrepancy between single-electron and Fe^{55} measurements indicates that CF_4 may have serious electron attachment. The gas gain from single electrons was about 5 $\sim$ 12 times higher than that from Fe^{55} in Ar/CF_4 (80/20). Other gas mixtures containing CF_4 show similar behaviour, though the discrepancy may be not as big as for Ar/CF_4. Among the mixtures studied $Ar/CF_4/C_2H_2$ (70/10/20) shows smallest discrepancy. Further studies of different gas mixtures containing CF_4 are certainly needed to identify the one which has the smallest electron attachment.

Additional evidence for electron attachment is the poor energy resolution observed in gas mixtures containing CF_4. Previous work [16] yielded energy resolutions with Ar/CF_4 (95/5) and (90/10) of $\sim$ 60% and $\sim$ 75%, respectively. We have measured the energy resolution for several conventional drift-chamber gases and also for gas mixtures containing CF_4. Typical values are summarized in Table 1, and some spectra are shown in Fig. 15.

There appears to be little or no dependence of energy resolution on gas pressure for the conventional drift-chamber gas mixtures, and in all cases we found resolutions better than about 18% for the 5.9 keV x-rays.

For all of the gas mixtures containing CF_4 the measured energy resolution is worse than this, and worsens with increasing gas pressure and with increasing percentage of CF_4. We plot the energy resolution of Fe^{55} x-rays *vs.* the ratio of gas gains initiated by single-electron and Fe^{55}, G_{Se}/G_{Fe}, in Fig. 16. The data points can be fitted by a straight line on the log-log plot, with slopes for many different gas mixtures all very close to 0.5. We interpret this as evidence that

$$\left(\frac{\sigma_G}{G}\right)^2 \propto \frac{1}{n},$$

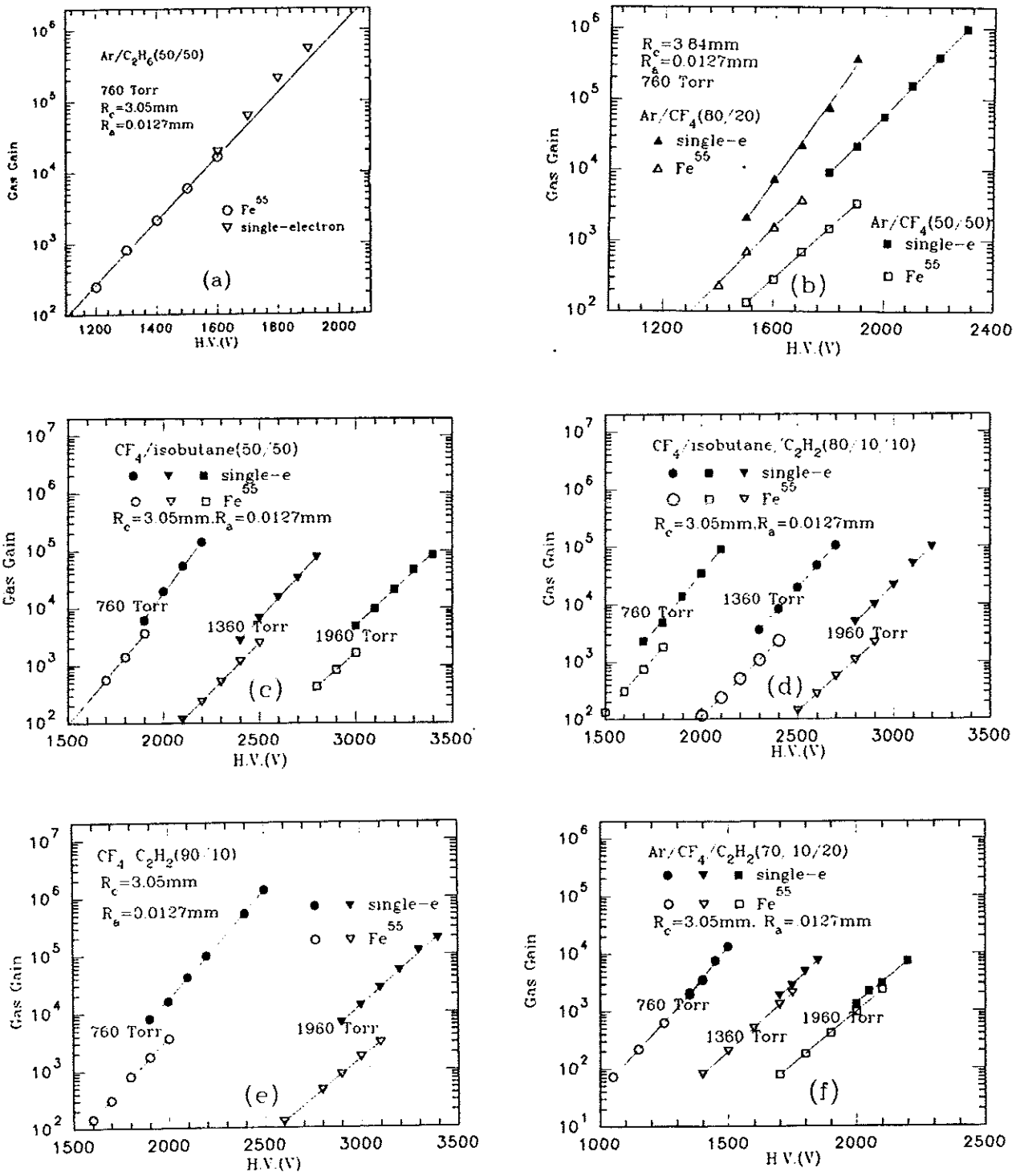

Figure 14: Gas gain from single photoelectrons and from Fe^{55} x-rays in (a) $Ar/C_2H_6(50/50)$, (b) Ar/CF_4, (c) CF_4/isobutane, (d) CF_4/isobutane/C_2H_2, (e) $CF_4/C_2H_2(90/10)$, (f) $Ar/CF_4/C_2H_2$.

Table 1: Energy resolution of various gas mixtures using an Fe^{55} source.

	P (torr)	Gas Gain	Resolution (Fe^{55})
Ar/CH_4			
90/10	760	217	14.6%
	1360	301	15.3%
	1960	148	15.5%
Ar/C_2H_6			
50/50	760	440	16.3%
	1960	253	16.3%
Ar/isobutane			
80/20	760	206.0	16%
	1160	377.1	18.4%
	1960	243.8	17.3%
90/10	760	188.5	13.3%
	1160	2564.0	12.5%
	1960	1861.0	15.2%
Ar/CO_2			
50/50	760	308	15.0%
	1360	284	18.5%
	1960	344	17.3%
Ar/CF_4			
80/20	760	98.8	48%
	1160	105.9	61%
	1960	107.2	82%
50/50	760	119.0	53%
	1160	92.2	63%
	1960	89.1	98%
CF_4/isobutane			
80/20	760	2089	33.9%
	1060	2100	37.4%
	1960	1241	46.8%
60/40	760	1709	22.9%
	1160	1544	26.1%
	1960	1426	31.6%
50/50	760	1297	21.5%
	1160	1106	22.3%
	1960	1580	26.9%

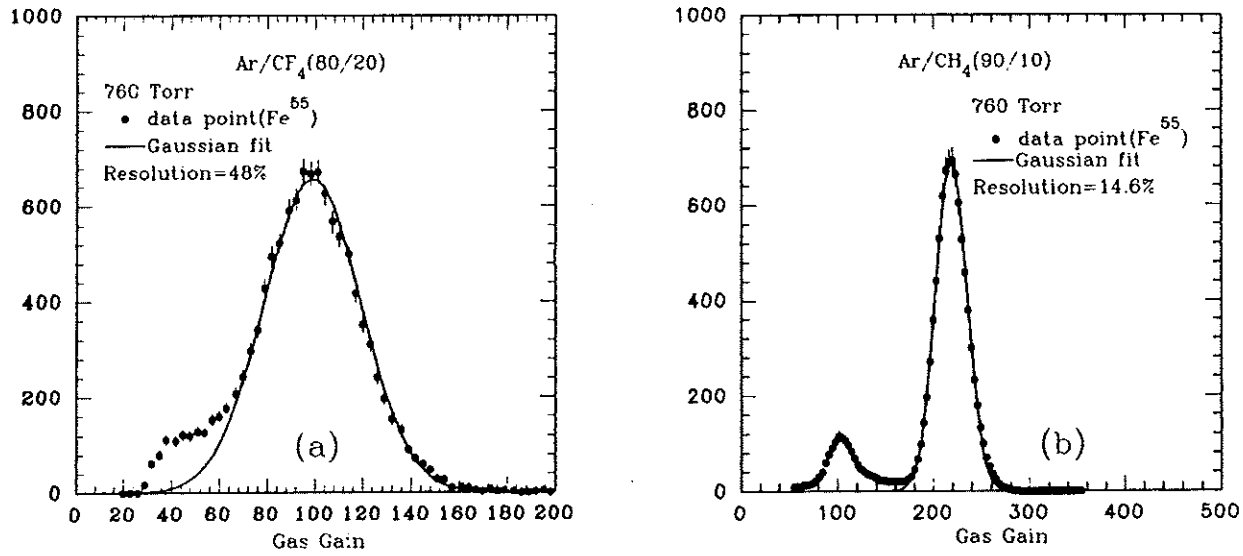

Figure 15: Gas-gain spectra in Ar/CF_4 and Ar/CH_4 mixtures using an Fe^{55} source.

where n is the number of electrons that do not become attached. Extrapolating to $G_{Se}/G_{Fe} = 1$, *i.e.*, to the limit of no attachment, we find an energy resolution of $\sim$ 18% just as for gases that do not attach electrons.

For the third evidence of electron attachment we examined the ratio of the number of detected single electrons N_c to the number of laser pulses N_t. This ratio is proportional to the detection efficiency for single electrons. If there were no electron attachment, this ratio should be constant for different gas pressures provided that the laser beam intensity is unchanged.

We plot N_c/N_t *vs.* P in Fig. 17(b) for CF_4/C_2H_2 (90/10) and Fig. 17(c) for Ar/C_2H_6 (50/50). The different pressure dependence of this ratio for Ar/C_2H_6 and CF_4/C_2H_2 is a clear indication of electron attachment in CF_4/C_2H_2.

1.2.7 Model of Electron Attachment in a Straw Tube

The mean free path, $1/\eta$, for electron attachment in pure CF_4 has been measured [22] with the results as shown in Fig. 18 for η/P *vs.* E/P. There is a crossing point for α/P and η/P, where α is the Townsend coefficient. When the reduced electric field E/P is below this point, the loss of drifting electrons due to attachment is greater than the gain due to Townsend multiplication. Above this point the Townsend multiplication will dominate over the attachment.

The basic mechanism of electron attachment in CF_4 is dissociation of the molecule into $F^- + CF_3$, $F^- + F + CF_2$, or $F + CF_3^-$, *etc.*, for which the electron-energy threshold is about 5 eV [16]. Thus the dissociation energy is less than the ionization energy for electron multiplication, so the attachment takes place outside the gain region. Still, the drifting electron must have gained considerable energy before is can dissociate the CF_4, so

Table 1: Energy resolution of various gas mixtures using an Fe^{55} source (*continued*).

	P (torr)	Gas Gain	Resolution (Fe^{55})
CF_4/C_2H_2			
90/10	760	1078.7	38.7%
	1960	1647.0	44.8%
CF_4/isobutane/C_2H_2			
80/10/10	760	310	31.9%
	1360	502	36.9%
	1960	274	49.5%
70/10/20	760	225	25.5%
	1360	162	32.0%
	1960	361	39.5%
$Ar/CF_4/C_2H_2$			
80/10/10	760	280	18.0%
	1360	309	19.7%
	1960	200	21.7%
70/10/20	760	218	19.4%
	1360	202	21.4%
	1960	409	21.3%

the attachment occurs in the higher-field region near the anode wire.

Therefore we can divide the whole cylindrical drift region into three areas, as shown in Fig. 19. In region 1 the electron energy is too low to dissociate the CF_4. In region 2 the electron will be possibly lost. In region 3 the electron can still dissociate CF_4 molecules, but it can also eject electrons from the CF_4 with greatly probability. According to this simple picture, the only region which need to be concerned about for the degradation of the efficiency is region 2. For different-sized drift tubes with same diameter anode wire operating at the same gas gain, the extent of region 2 should be similar, and so also the amount of electron attachment.

Assuming the depth of region 2 to be denoted as d, the initial number of electrons as n_0, and the surviving number of electrons after crossing region 2 as n, it follows that

$$\frac{n}{n_0} = e^{-P\int_{r_1}^{r_2}(\eta/P)dr},$$

where $r_2 - r_1 = d$. For a given gas mixture η/P will be the function of E/P only, therefore

$$\frac{1}{P}\ln\left(\frac{n}{n_0}\right) = F(E/P),$$

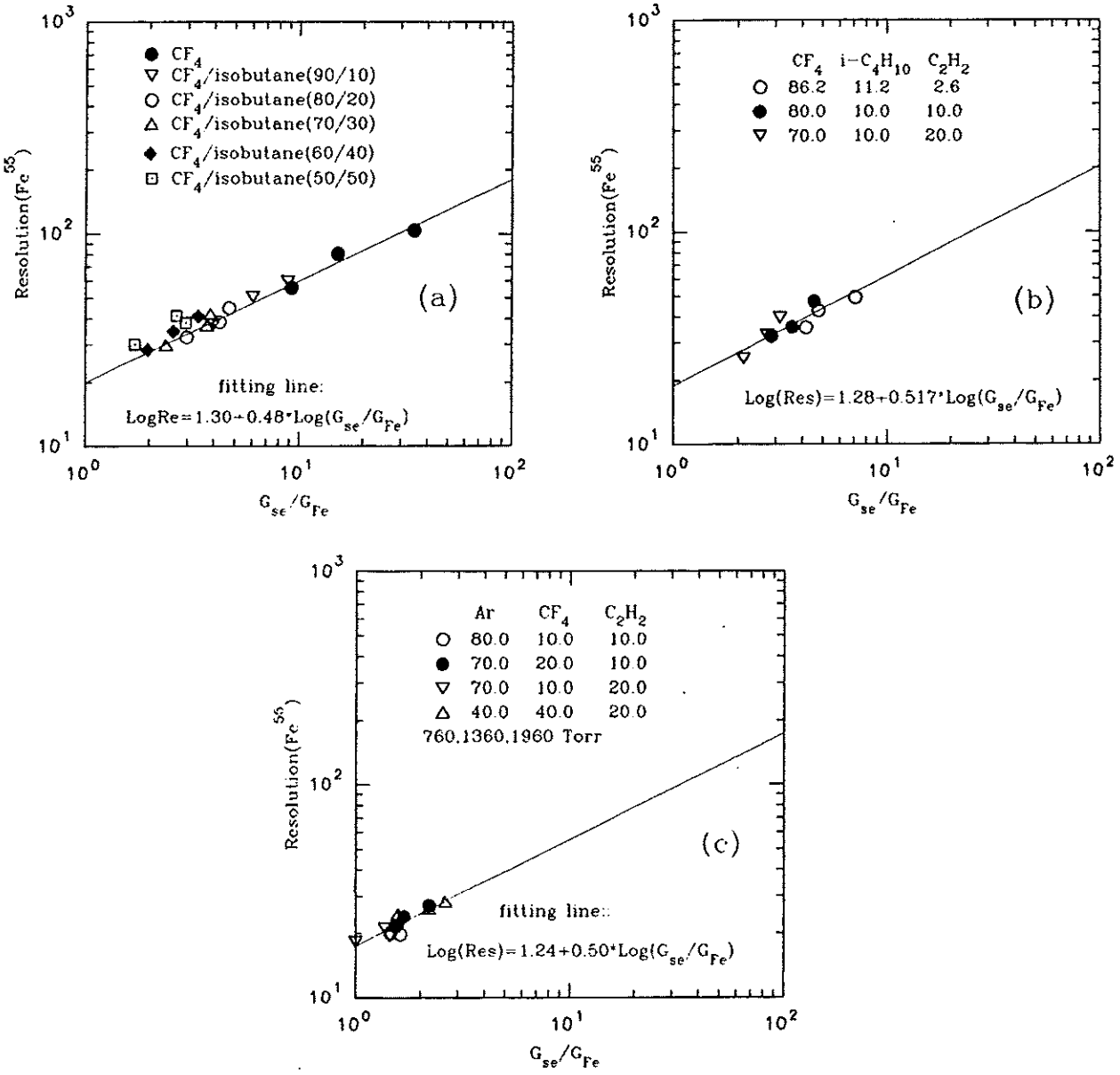

Figure 16: Energy resolution of Fe^{55} x-rays *vs.* G_{Se}/G_{Fe}. (a) CF_4/isobutane, (b) CF_4/isobutane/C_2H_2, (c) Ar/CF_4/C_2H_2. For each gas mixture, the three data points represent three different pressures, 760, 1360, and 1960 torr, from left to right, respectively.

The electric field in a straw tube varies as $E/P = V/[Pr\ln(R_c/R_a)]$, where V is the high voltage on the anode wire, R_c, and R_a are the radii of cathode and anode, respectively, r is the distance from the center of the tube. Hence we expect $(1/P)\ln(n/n_0) = F\{V/[PR_2\ln(R_c/R_a)]\}$, where R_2 is some characteristic radius of region 2.

To test this expression we installed three different size of drift tubes into the test cell,

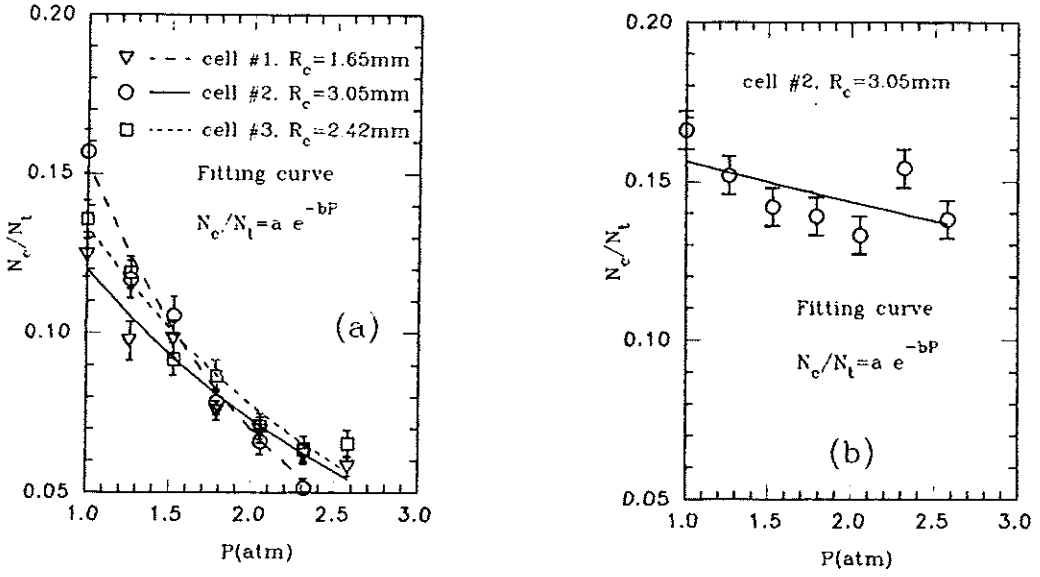

Figure 17: Electron attachment *vs.* gas pressure. (a) CF_4/C_2H_2 (90/10), (b) Ar/C_2H_6 (50/50).

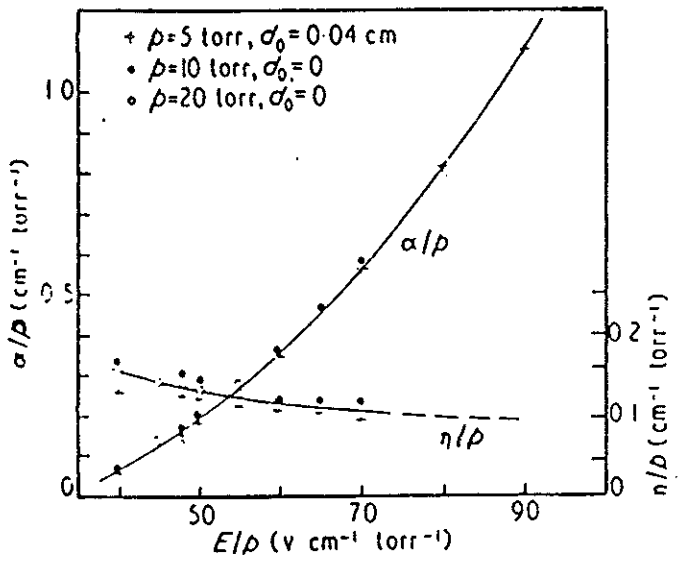

Figure 18: Townsend and attachment coefficients in CF_4 [22].

with cathode radii of R_c = 1.65, 2.42, and 3.05 mm. These three tubes had same diameter anode wire, and shared the same gas volume. Using the N_2 laser we recorded the number of laser pulses N_t and the number of detected single photoelectrons N_c. We plot $(1/P)\ln(N_c/N_t)$ *vs.* $V/[P\ln(R_c/R_a)]$ for the three drift tube under several different gas pressures in Fig. 20. Supposing that the characteristic radius R_2 of region 2 is the same in all

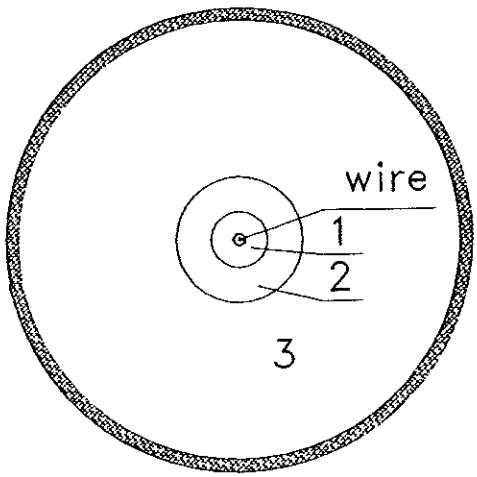

Figure 19: Three different regions inside of a drift tube. Gain dominates over attachment in region 3, attachment over gain in region 2, and in region 1 there is neither attachment or gain.

cases, all of the data points should fall into the same smooth curve. The data appear to support this.

From Fig. 18 we take $\eta/P \simeq 0.1$ cm-torr as a constant. Then our model calculation implies

$$\frac{N_c}{N_t} = e^{-(\frac{\eta}{P}d)P}.$$

From either Fig.17 or Fig. 20 we infer that the size d of region 2 is about 80 μm. Also from Fig. 18 we infer that the inner radius of region 2 occurs when $E/P \sim 45$ V/(cm-torr). For the case that $V = 2000$ volts, $P = 760$ torr, and $R_c/R_a = 3/0.01$, this inner radius would be 100 μm.

When a similar study is made with Ar/C_2H_6, as shown in Fig. 17(b), there is little evidence of electron attachment.

1.2.8 Effect of Electron Attachment on Position Resolution

Assuming the timing of the straw-tube chamber is based on the detection of the first arriving electron, we have made a simple Monte Carlo calculation that estimates the effect of electron attachment on the position resolution.

When a minimum-ionizing particle goes through the straw tube, it leaves several primary clusters in the gas. The number of clusters will be distributed according to Poisson's law. The mean number of primary clusters for gas mixtures containing CF_4 is taken to be 4.1/mm, and the mean number of electrons in a cluster is 3 [17]. The position distribution of these primary clusters along the particle's track is be $f(x) = e^{-x/\lambda}/\lambda$, where $\lambda = 1/(4.1$ mm).

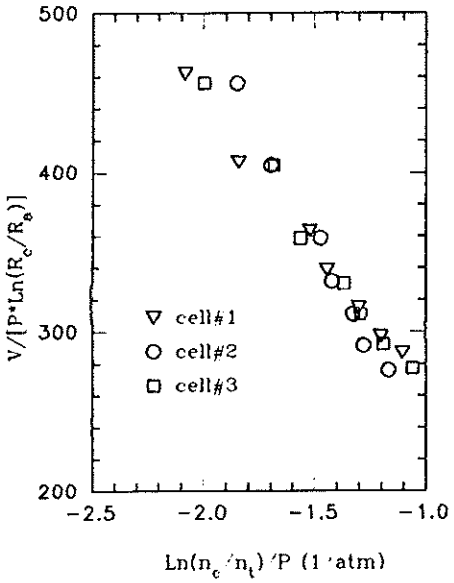

Figure 20: Test of the model of attachment in region 2 of a straw tube.

Due to fluctuations of primary cluster position, the shortest distance an ionization electron travels is be longer than the impact parameter between anode wire and the track, and also has a distribution. The inefficiency of electron's detection due to electron attachment will further widen this distribution. The width of this distribution limits the precision of the position measurement.

In Fig. 21 we plot σ of this distribution *vs.* the impact parameter for ten different detection efficiencies and for three different sizes of straw tube (R_c = 1.5, 2.0, and 2.5 mm). We see that the position resolution will degrade abruptly when the single-electron detection efficiency becomes less than 0.4. According to our measurements the efficiency for single electrons could be as low as 10% for some gas mixtures containing CF_4. However, except when the single-electron detection efficiency is as low as 0.1, the detection efficiency for any electron from the primary ionization is not seriously affected by the electron attachment, as shown in the lower part of Fig. 21.

1.2.9 Measurement of the Gas Coefficients $\alpha - \eta$

In the previous sections we have summarized nearly all the work done in FY91 on the characterization of single-electron avalanches. Some aspects of this work remain to be done, and we propose to continue these studies in FY92. We will make four additional types of measurements:

1. Measurement of the difference between the Townsend coefficient α and the attachment coefficient η.

2. A measurement of another combination of α and *eta* to separate the two quantities.

3. Measurement of the electron drift velocity.

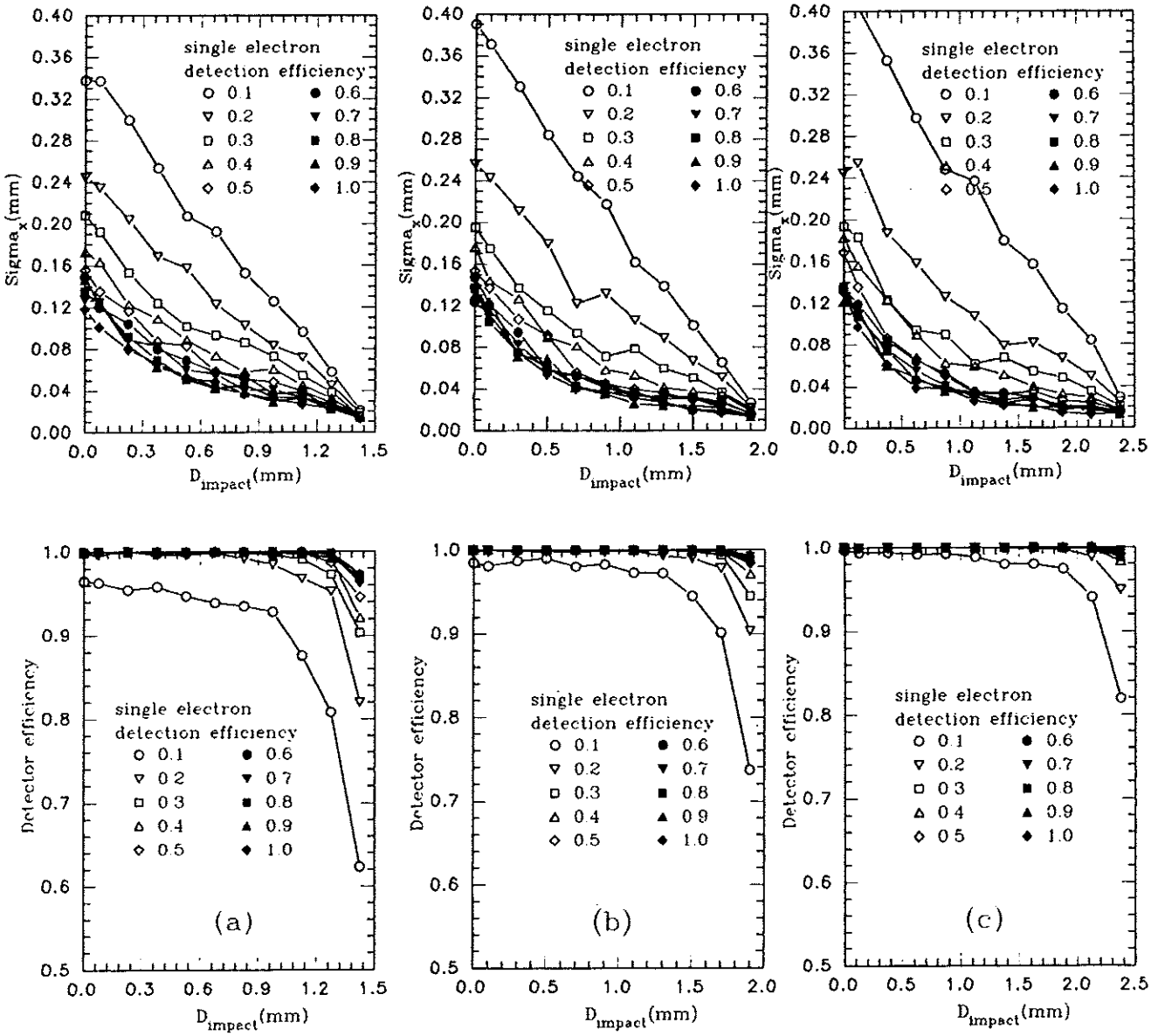

Figure 21: Effect of electron attachment on the position resolution (upper plots), and on overall track efficiency (lower plots). (a) R_c = 1.5 mm, (b) R_c = 2.0 mm, (c) R_c = 2.5 mm.

4. Measurement of the primary ionization density, and the number of electrons per primary ion cluster.

Some preliminary work on measurement of $\alpha - \eta$ has already been performed, using the set-up shown in Fig. /reffig91. A large N_2 laser pulse ejects n_0 electrons from the cathode of a parallel-plate chamber. This chamber can be operated at low pressure to achieve the

large values of E/P found near the anode wire of a straw-tube chamber. As the electrons drift across the large chamber gap they may be attached, and they may also cause Townsend multiplication. The number of surviving electrons is

$$n_e = n_0 e^{(\alpha-\eta)d},$$

where d is the chamber gap. In addition, the negative ions created by electron attachment also drift towards the anode.

The signal of the n_e electrons is detected in a second parallel-plate chamber separated from the first by a 80%-transparent wire mesh. The second chamber gap is operated at a voltage that provides a significant gas gain. Because the heavy negative ions from electron attachment do not participate in electron multiplication in the second chamber gap, the signal on the anode there is essentially that due to the n_e surviving electrons from the first gap.

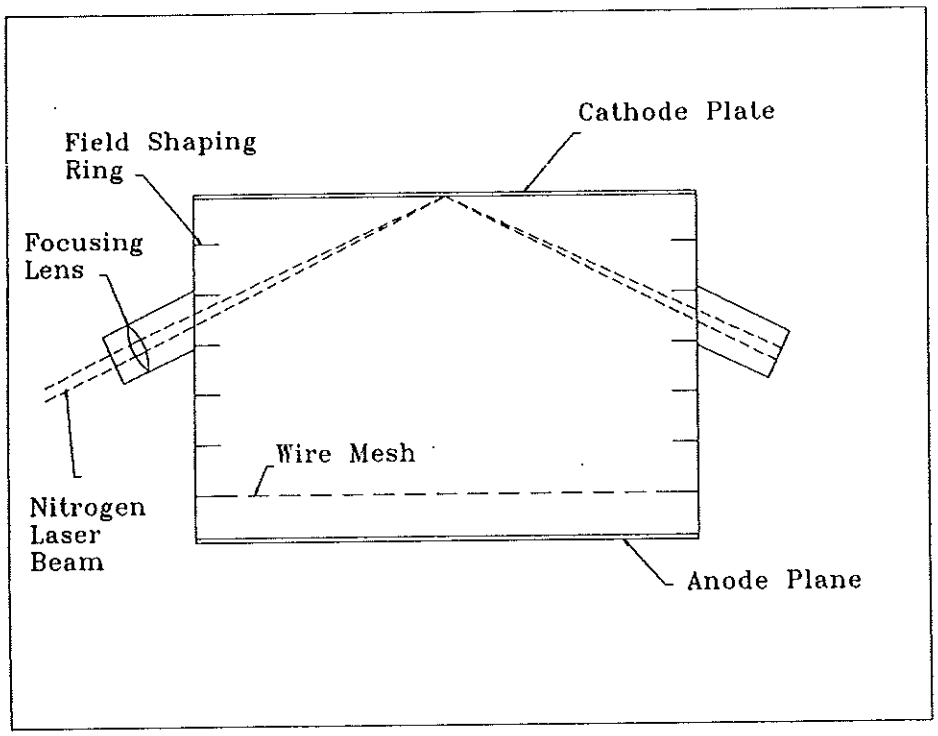

Figure 22: Set-up to measure $\alpha - \eta$.

Data are collected at various values of electric field E and pressure P. We plot the values of $(\alpha - \eta)/P$ so deduced against E/P and expect a single curve for a given gas mixture.

Our present chamber has a small leak and must be rebuilt in stainless steel. Nonetheless, preliminary results, shown in Fig. 23, indicate that the technique is close to success. The plot for P-10 gas shows only positive values of $\alpha - \eta$ as expected for a gas mixture with little attachment. The plot for CF_4 indicates that attachment becomes significant for $E/P \sim$ 15 V/(cm-torr), but that multiplication exceeds attachment once $E/P \gtrsim 40$ V/(cm-torr). Previous work (Fig. 18) suggests a value of $E/P \sim 45$ when multiplication dominates.

Note that our chamber has sufficient range of E/P to see both the low and high values of this parameter for which attachment dominates.

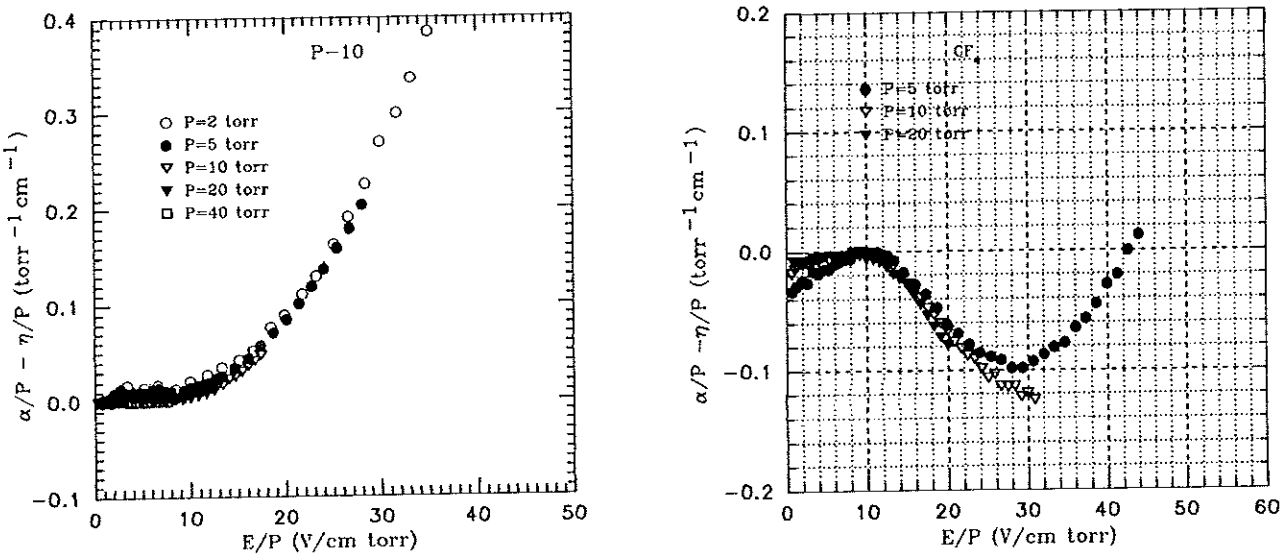

Figure 23: Preliminary measurement of the gas coefficients $(\alpha - \eta)/P$ as a function of E/P for (a) P-10, and (b) CF_4.

1.2.10 Proposed Measurement of Another Combination of α and η

To extract separate values of the Townsend coefficient α and the attachment coefficient η, we need a measurement of another function of these two quantities.

A proposed set-up for this is shown in Fig. 24. Here a single-gap parallel-plate chamber has electrons ejected from the cathode by a continuous UV lamp. In this configuration we collect both the n_e surviving electrons, and the n_i negative ions fur to electron attachment. The latter are created according to

$$dn_i = \eta n_e dx.$$

On integrating over the gap size d using the previous expression for n_e, the total charge collected at the anode is

$$n = n_0 \frac{\alpha e^{(\alpha-\eta)d} - \eta}{\alpha - \eta}.$$

Because the negative ions drift much more slowly than the electrons it is preferable to use a continuous UV source and observe the current off the anode, rather than integrating the charge from a pulsed source. By varying the gap d as well as E and P a thorough measurement of a second function of α and η will be made.

1.2.11 Proposed Measurement of the Drift Velocity

For a self contained study of chamber gases it is important that we measure the drift velocities in our gas mixtures, rather than relying on the somewhat sporadic literature.

A proposed set-up for this is shown in Fig. 25. The apparatus is similar to that shown in Fig. 22 in that the photoelectrons drift across a large parallel-plate chamber before being

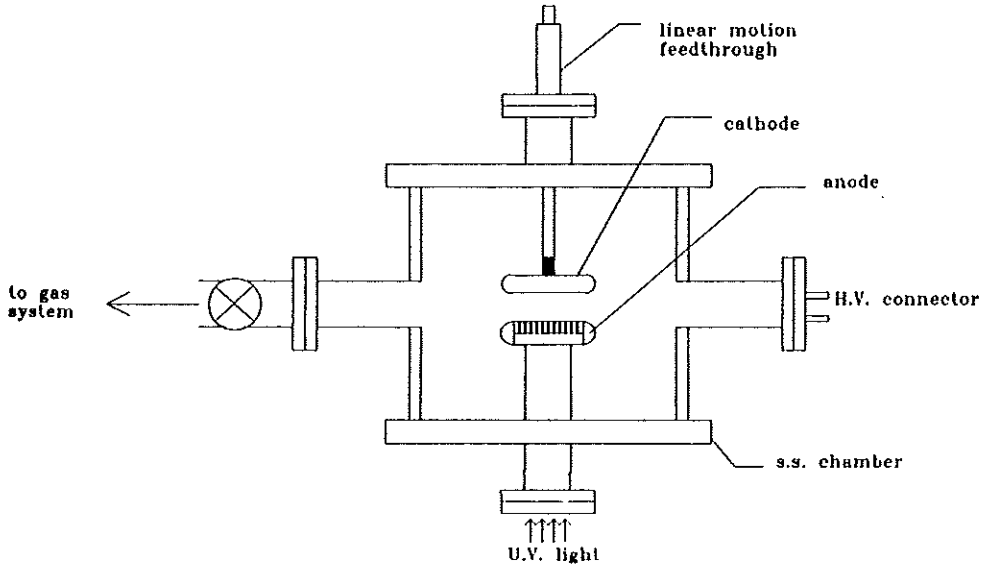

Figure 24: Set-up to measure a second function of the gas coefficients α and η.

detected in a second, amplifying gap. While the time of photoemission by the N_2 laser pulse is well known, only the sum of the drift times across the first and second gaps is measured by timing of the output pulse from the second chamber. To measure the drift time across the second gap, we will evaporate a thin layer of aluminum on the wire mesh that separates the first and second chamber gaps. Then there will be a small signal of photoelectrons from this mesh created essentially simultaneously with the emission of electrons from the cathode. By measuring the time difference of the two pulses on the anode of the second gap, the drift time across the first gap can be determined.

As with our previous double-gap chamber, very large values of E/P can be achieved, so we can measure the drift velocity over the complete range of parameters relevant to a cylindrical proportional chamber. Most data in the literature is restricted to low values of E/P.

1.2.12 Proposed Measurement of Primary Ionization Density and Cluster Size

The last set of measurements we propose is that of the primary ionization density caused by minimum-ionizing particles, and the associated cluster size.

For this the set-up will be essentially as in Fig. 22, but using cosmic rays as the source of charge separation in the chamber. By using very low electric field in the main gap, the time of arrival of individual clusters at the anode can be resolved. The signal will be sampled by a transient digitizer (digital oscilloscope) whereby the size of each cluster can be separately determined. [This is the familiar principle of the time-expansion chamber.]

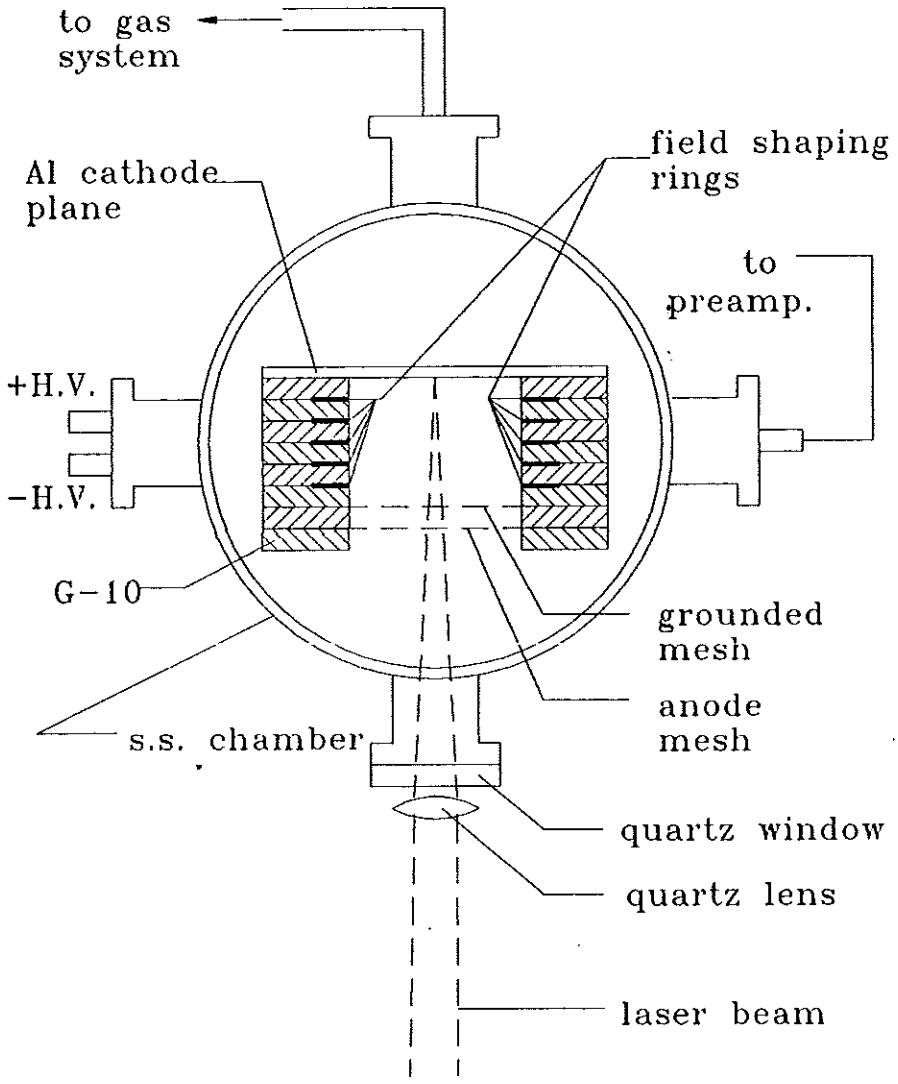

Figure 25: Set-up for measurement of drift velocity.

1.3 Prototype Straw-Tube System

We have constructed a set of three prototype straw-tube modules (Fig. 26) each containing an 8×8 bundle of straws, for a total of 192 channels. The channel count was determined by the available number of U. Penn-AT&T preamps. At the time of this writing final bench tests of the system are being made, and we plan to take the system to the Fermilab M-Test beam in the near future.

1.3.1 Mechanical Construction

The present prototype modules do not address issues of long straws, and the straw length is only 30 cm. The inside diameter of the straws was 0.275 inches (7 mm) to be compatible with end plugs based on the design of an Ohio State U. group [23].

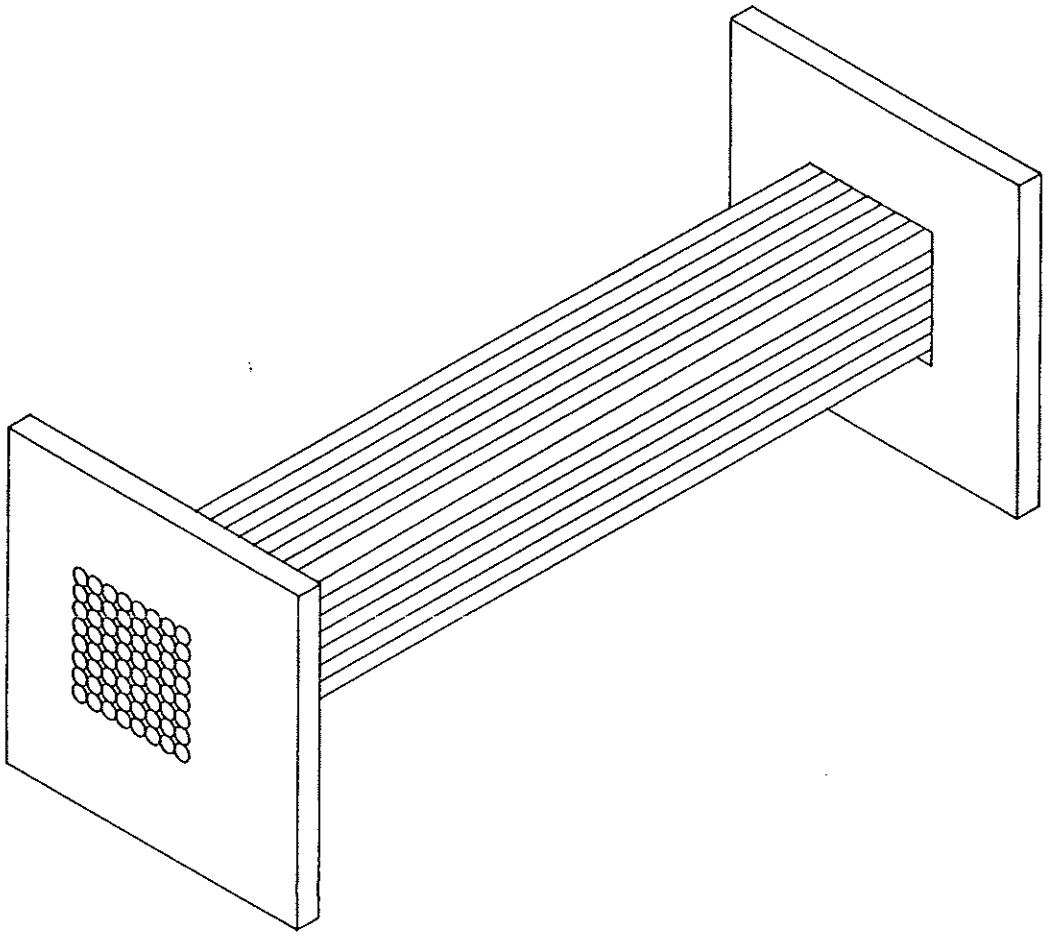

Figure 26: View of an 8×8 bundle of straw tubes, each 30-cm long and 7 mm in diameter. The actual bundle is on a hexagonal-close-pack lattice, rather than on a rectangular lattice as shown here.

The straw tubes were wound by Stone Industrial from an inner ply of 0.6 mil Makrofol carbon-loaded polycarbonate (Mobay Co.) and an outer ply of 0.5 mil Mylar. The polycarbonate film was aluminized by Sheldahl Co. to about 1000-Å thickness, corresponding to a surface resistivity of about 1 ohm/□. The polycarbonate film has a surface resistivity of about 500 ohm/square to minimize the effect of possible scratches to the aluminum layer in handling of the tubes [23]. As a further protection, the tubes were wound with an internal 'slip sheet' of Nomex that was removed just prior to use.

While the straw tubes can withstand more than 10 atmospheres of internal pressure, they are too thin to be mechanically sound when not pressurized. This presents a problem when the straws are to be glued together into a bundle. Rather than use steel mandrels inside the straws during the gluing [23], we devised temporary end plugs that permit the straws to be pressurized for gluing. The temporary end plugs consist of an aluminum insert and a bicycle-tire valve (Schrader Co.) mounted in a brass collar that screws onto the aluminum

insert, as shown in Fig. 27. The latter is part of the final end-plug assembly, and is glued to the straw end with conducting epoxy.

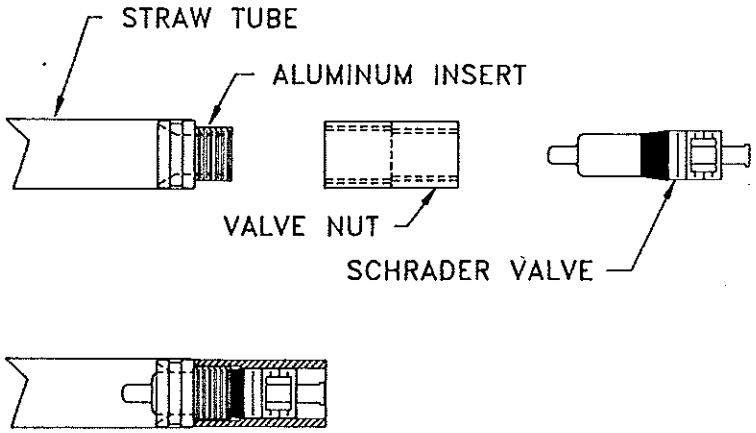

Figure 27: The temporary end-plug assembly. The brass collar containing a bicycle-tire valve is screwed onto the threads of the aluminum insert so the straw tube can be pressurized for gluing in the straw-tube bundle. Later the brass collar is removed, and the threaded region of the insert engages the alignment hole on the aluminum end plate.

The pressurized straws were laid one by one into an alignment fixture. As each additional straw is added to the bundle, those portions of its azimuth that would come in contact with the existing bundle were coated with a thin layer of 5-minute epoxy. This was applied with a special roller to minimize the build-up of epoxy. The triangular space between three osculating straws remained largely free of epoxy.

When a bundle of 64 straws was complete and the epoxy dried, the brass collars with the bicycle valves were removed. At this point the bundle could be handled, though with some risk of indenting the outer layer of straws.

The next phase of construction was the stringing of the anode wires, which are 0.8 mil gold-plated tungsten from Luma Metal, chosen for its excellent surface finish (as can be confirmed with an electron microscope). The wire tension was 45 gm, only about 50% of the breaking strength of the wire.

First, the straw tube bundle was epoxied to a 0.125-inch-thick aluminum end plate with holes machined to match the aluminum inserts discussed above. The conducting epoxy provided a both a gas seal and electrical connection to the straw-tube walls.

Next, the Ultem feedthroughs (Fig. refpfig3) were inserted into the aluminum inserts. The fit is tight and some care is required to insert the feedthrough without damage to the epoxy joint. The Ultem feedthroughs contain a precision V-groove to position the wire during and after stringing. Due to an accident at the vendor (McCourtney Plastics) the mold for the feedthroughs was out of tolerance and the V-groove slightly off center. Nonetheless, we decided to accept the feedthroughs, and mount them at 180° azimuth on either end of the straws to insure the wire at least went through the center of the straw tube.

In the Ohio State scheme the anode wire is pinned to the Ultem feedthrough by the friction of a tapered brass pin (Fig. 29). We had considerable trouble getting the pins to

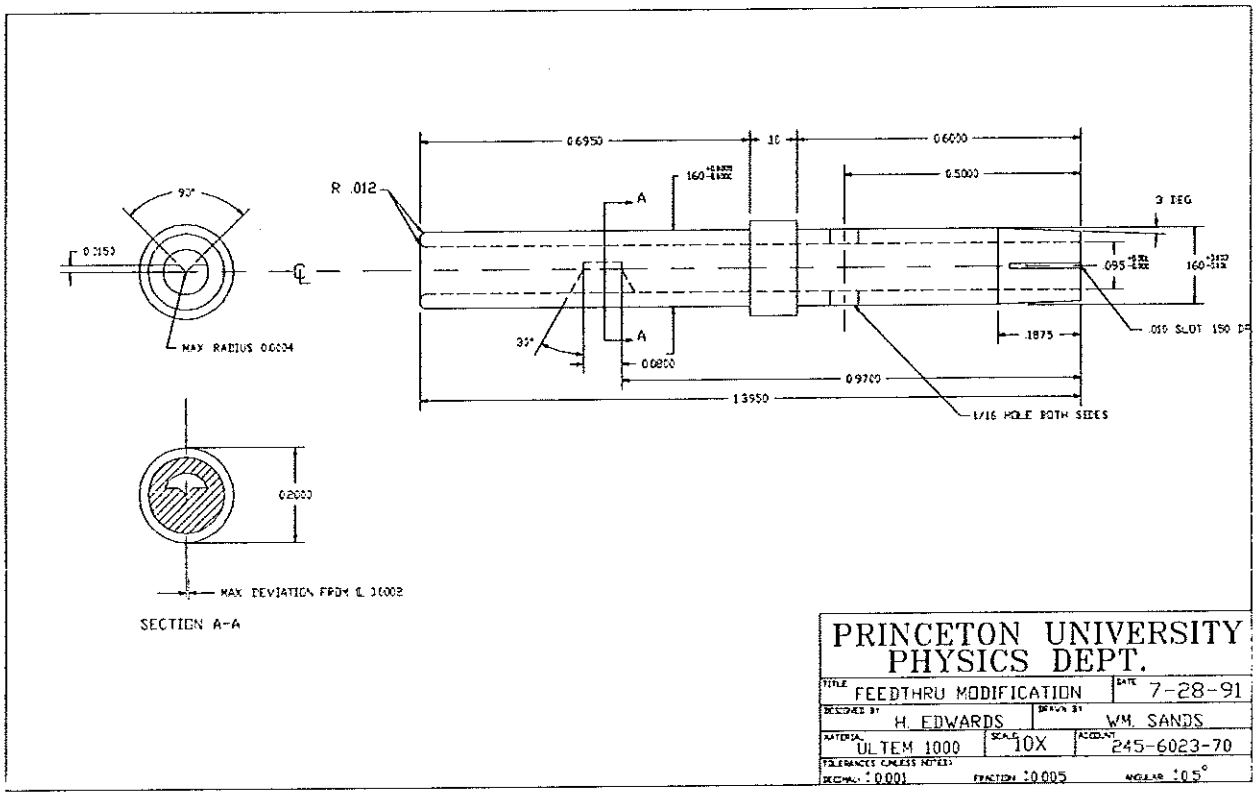

Figure 28: The Ultem feedthrough whose left end fits inside the aluminum insert (Fig. 27). The V-groove aligns the anode wire. Gas enters the straw tube through the two transverse holes in the feedthrough near is midpoint. The brass taper pin (Fig. 29) is inserted into the right end of the feedthrough to fix the anode wire.

stick without applying so much force that the tension in the wire was relieved in the process. Instead, we cut a small groove in the taper pins so the wire was no longer grabbed by the pin, and then we soldered the wire to the pins when the desired tension was achieved.

1.3.2 Measurement of the Wire Tension

In view of the anticipated difficulty in maintaining accurate wire tensions during assembly, we constructed a wire-tension monitor [9] that can be operated by the technicians who do the stringing, providing a measurement of the tension immediately after each wire is strung.

The straw-tube bundle is placed between the pole of a magnet, and a sawtooth current pulse is applied to the test straw via an arbitrary waveform generator (Markenrich Co.) that resides on the bus of a PC-clone computer. The resulting vibrations in the wire cause an induced e.m.f. that is detected by a digital oscilloscope card also in the PC. The set-up is illustrated in Figs. 30 and 31.

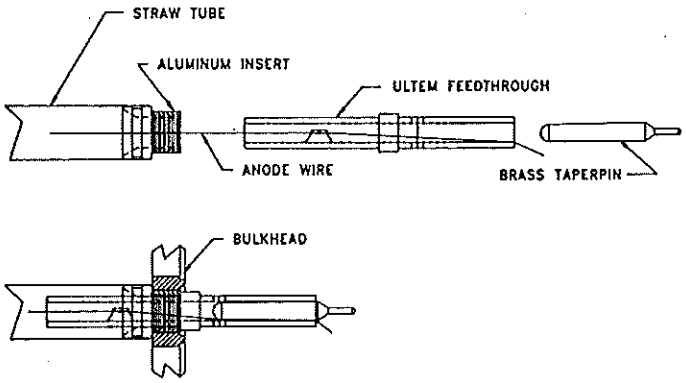

Figure 29: The final end-plug assembly consists of an Ultem feedthrough that fits inside the aluminum insert, and a brass taper pin that is inserted into the Ultem feedthrough to fix the anode wire.

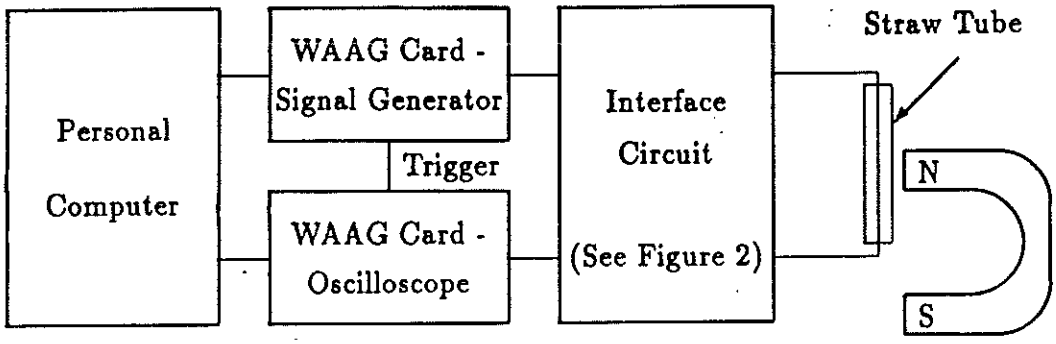

Figure 30: Block diagram of the apparatus to measure the wire tension

The sawtooth pulse builds up over 0.1 s causing the anode wire to be pulled to one side by the interaction with the magnetic field. As the magnetic field region is less than the wire length, the spatial configuration of the perturbed wire is triangular. Then the sawtooth pulse drops to zero in less than a millisecond, exciting a vibration in the anode wire much like the plucking of a banjo. Fourier analysis of the triangular initial condition shows that only odd harmonics are excited, with relative amplitude of $1/n^2$ for the nth mode.

The induced e.m.f. depends on the velocity of the wire rather than its amplitude, so the series expansion of the e.m.f. has only odd harmonics with strength $1/n$, *i.e.*, a square wave. Figure 32 shows a typical induced-e.m.f. signal as recorded on the digital oscilloscope.

The computer detects the zero crossings of the waveform and deduces its fundamental frequency ν in about 10 seconds. The waveform is actually damped in time, as seen in Fig. 32, and the decay constant γ is also determined by the computer. The wire tension is then obtained from

$$T = 4(\nu^2 + \gamma^2)\rho L^2,$$

where ρ is the linear mass density of the wire, and L is its length. The accuracy of the

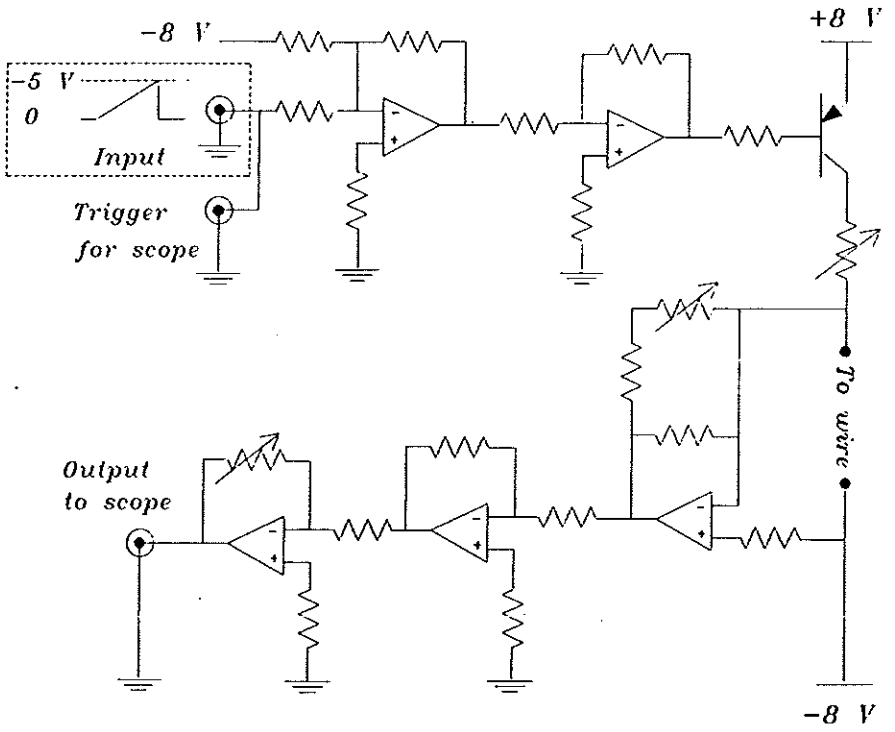

Figure 31: The interface circuit for the wire-tension monitor. This amplifies the output of the waveform generator, and also amplifies the induced e.m.f. across the wire.

measurement is limited by the noise of the electronics, which leads to an accuracy of about 0.5% on the tension, as inferred from the spread of a set of repeated measurements.

1.3.3 Preamplifier Cards

The readout electronics are base on the U. Penn bipolar preamplifier chip [12] that has recently become available in small quantities. This chip is implemented in an AT&T semi-custom bipolar process to obtain a 3-ns rise time when operating at about 20 mWatt power. The version presently available comes in a 16-pin surface mount package, and does not include a discriminator/shaper as should be part of future versions. In a single channel test set-up we have confirmed that stated noise specification of about 1100 equivalent electrons.

To match the packing geometry of our straw-tube bundles, we have built an 8-channel preamplifier card. The circuit is shown in Fig. 33, and the board layout shown in Fig. 34. The pc board is two layer, with surface-mount components throughout. The boards were manufactured and components installed by T.L. Industries.

The U. Penn chip has dual inputs as well as a signal return. The pin-12 input is used by use for the signal, while the pin-15 input, which is inverted with respect to pin 12, is the 'rf-reject' line. Ideally this line should extend along a physical path paralleling the signal path to provide a subtraction of currents induced on the signal line by sources outside the

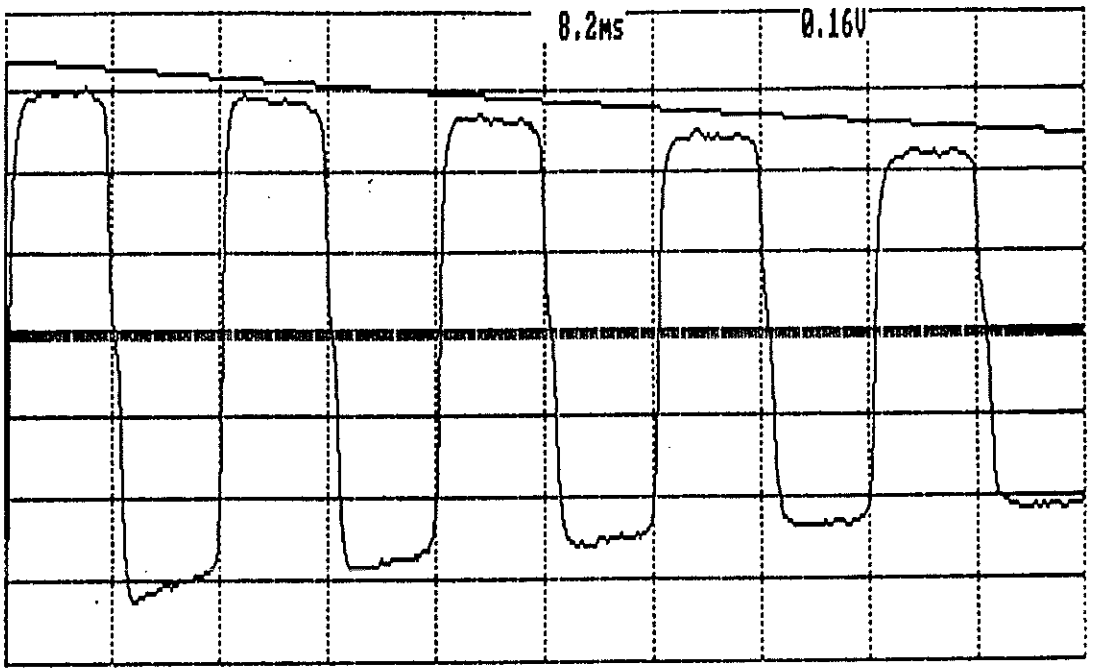

Figure 32: A waveform for the induced-e.m.f. signal as observed with the wire-tension monitor.

straw tube.

An Analog Devices 96685 comparator produces differential ECL outputs for the duration of the output of the U. Penn chip over an adjustable threshold. For diagnostic purposes we included an Analog Devices 848 buffer amplifier with unity gain that can drive the output waveform from the U. Penn chip into a 50-Ω line.

We find that our circuit oscillates for threshold below about 1 fC, or about six times the noise limit of an individual U. Penn chip. Future implementation of the circuit in a multilayer pc board should improve this.

1.3.4 Electrical Connections

The preamplifier cards are not connected directly to the straw-tube end plugs. The latter must be in a volume that contains chamber gas as they are part of the gas-distribution system. Also, in our configuration the straw tubes are at ground, and the anode wires at positive high voltage. Hence we need a high-voltage blocking capacitor between each end plug and preamplifier input. We have chosen to place the blocking capacitors inside the chamber-gas volume, so that no high voltage appears on the preamplifier card.

We have made two small pc boards, shown in Fig. 35 that attach to either end of a row of 8 straw tubes via sockets (not shown in the Figure) that engage the brass taper pins. Card b) has a 220 pF high-voltage capacitor on each line, manufactured by K.D. Components.

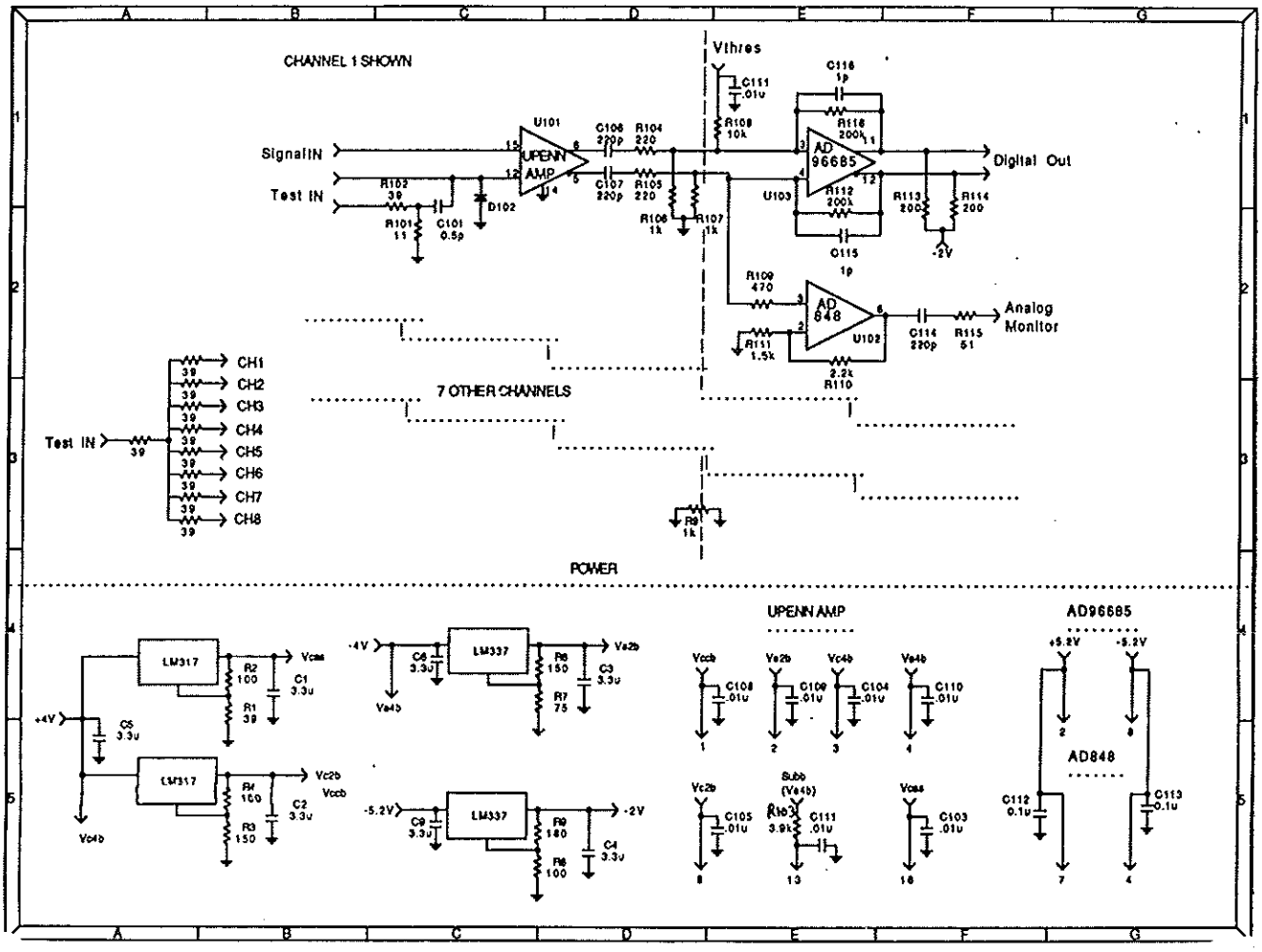

Figure 33: Circuit diagram of the preamplifier card.

The somewhat low capacitance of the blocking capacitor was chosen to minimize the stored energy that might damage the preamp in case of a wire snapping. The capacitor is a simple parallel-plate device with dimensions $1.5 \times 2 \times 4.5$ mm^3.

Card a) supplies the high voltage to each anode wire through an individual 10-MΩ surface-mount resistor, and can also terminate that straw tube in a 270-Ω resistor through a second high-voltage capacitor. The 10-MΩ resistors can stand off 3000 volts, so if an anode wire snaps the system can continue running.

As the high voltage is distributed to 32 straw tubes in parallel, the effective bleed resistance of 10/32 MΩ is too low to damp high-frequency oscillations. So we have an additional 40 M-Ω resistor in series.

Cards a) and b) are mounted in small enclosures at each end of the straw bundle, as shown in Fig. 36. The preamplifier cards are mounted in the larger enclosures. Because adjacent straw-tube layers are separated by only $7 \cdot \sqrt{3}/2 = 6$ mm, we could not place all preamplifier cards on the same end of the straw-tube bundle with an in-line configuration. Instead, we mount four preamplifier cards on each end of the straw-tube module.

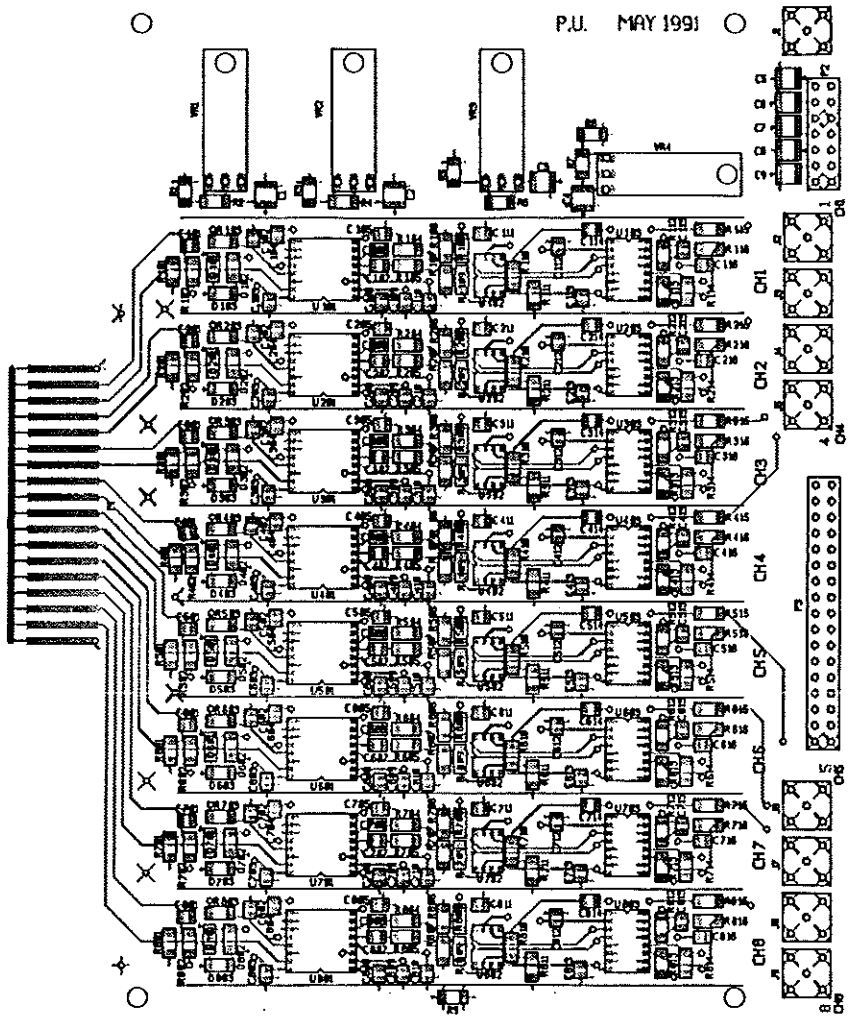

Figure 34: Component layout of the preamplifier card.

The signal return path is perhaps not ideal in our present geometry. The straw-tube cathodes are connected to the aluminum end plate. The latter attaches to the small-card enclosures and carries the signal return to the mounting plate of the preamplifier cards. From here we have straps that carry the signal return onto the bottom sides of Cards b) and hence onto the preamplifier cards. In addition we have straps that carry the signal return directly from the preamplifier mounting plate onto the preamplifier cards.

When the preamplifier cards are mounted on the chamber, they oscillate for thresholds lower than about 1.5 fC, at the present time. Work is in progress to improve the grounding, and shielding of the rather sensitive inputs to the U. Penn chips.

The preamplifier outputs are read into a LeCroy CAMAC TDC system based on their model 4291 32-channel TDC. The data will be collected onto disk with a 486 PC-clone computer. We have achieved a data-recording rate of 280 kbytes/sec.

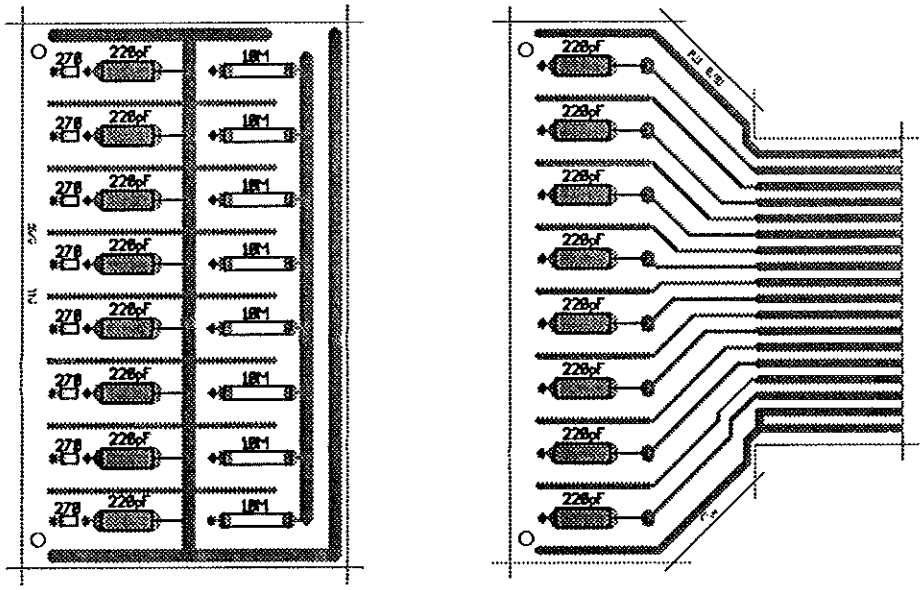

Figure 35: The small pc boards that connect to the straw tubes. Card a) distributes the high voltage, and terminates one end of the straw tube in 270 Ω. Card b) connects the straw tube to the preamplifier through a 220 pf high-voltage capacitor. The rf-reject line can be seen between neighboring signal lines.

1.3.5 System Test Program

In October 1991 we will use the three straw-tube prototype modules in the M-Test beam at Fermilab. In addition to providing a demonstration of a straw-tube system based on contemporary technology, this test will permit measurements of position resolution *vs.* impact parameter of a particle track. This complements our studies at Princeton using the N_2 laser to eject single electrons from a straw-tube wall.

We will seek a one-hour shift for data collection each day of running. In this time we should file our hard disk, which then requires about one hour to back up onto tape. The 23-hour down-time between data shifts will permit changing to a new chamber gas.

Once the Fermilab test is over we can continue the test program, if need be, back at Princeton using cosmic rays.

1.3.6 Proposed Phase-II Prototype Modules

In FY 1992 we propose to build a Phase-II prototype straw-tube system. This would explore three topics beyond the present system:

1. Modules with the longest straws that do not require internal supports for the anode wires. Based on our work in FY90, the length should be about 1.5-2 m for 7-mm-diameter tubes.

2. Coaxial connection of the straw-tube cathodes to the preamplifiers.

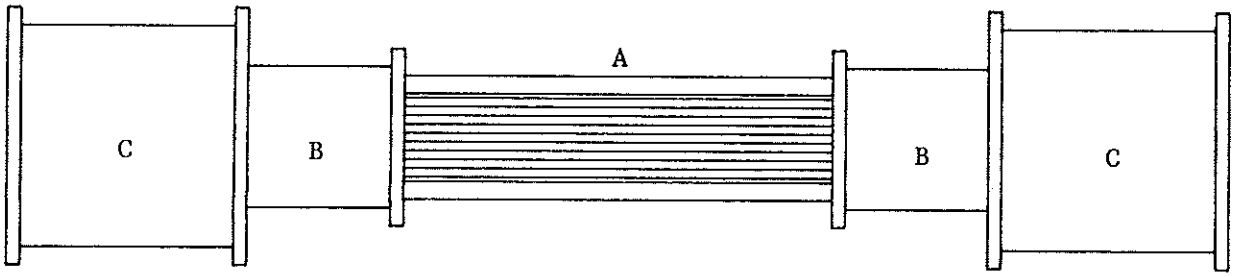

Figure 36: Side view of a straw-tube module showing the electronics enclosures. **A**: the straw tube bundle. **B**: the small enclosures containing Cards a) and b) and through which the chamber gas enters and exits the straw tubes. **C**: the large enclosures containing the preamplifier cards.

3. Implementation of the next generation of U. Penn bipolar preamplifiers. These will contain discriminator/shapers and be packaged four to a chip, permitting more compact electronics.

Topic 1, long straws, will include the use of straws with copper cathodes rather than aluminum, and likely the use of a Kapton substrate for the cathode, rather than the Makrofol polycarbonate film. A copper cathode will provide lower signal attenuation in long straws, better electrical contact with the end plugs, and a higher work function for suppression of UV feedback. There is also evidence [21] that copper cathodes have a longer mechanical life than thin layers of evaporated aluminum.

Topic 2, coaxial ground connections, is quite challenging. The very compact end plugs must stand off the high voltage, allow the chamber gas to flow, and provide a coaxial ground path. No more than two of these three requirements have been met in any design to date. We will redesign the aluminum inserts and the Ultem feedthroughs, as well as providing the functions of our Cards a) and b) on miniature PC boards in-line with each straw tube. There are sizable set-up costs for the manufacture of new inserts and feedthroughs, but these must be met to produce a significant advance in the end-plug performance.

Topic 3, utilization of new preamplifiers, is dependent on the pace of progress of the front-end electronics group at the U. Penn. We wish to note our strong support for this group, and encourage them to continue their excellent work into the next generation of bipolar chips, and into implementations of a TVC chip for on-chamber use.

2 Budget Proposal for FY92

In FY92 we propose to continue our characterization of single-electron avalanches as discussed in Secs. 1.2.10-1.2.12, and to construct a Phase-II prototype straw-tube system as outlined in Sec. 1.3.6. For this we propose a budget of $213k as detailed below.

1. Permanent Equipment

    1. Pumping station (Hovac BH2-60) $8k
    2. High-purity gas filters (Semi Gas) $3k
    3. Stainless-steel test chamber $5k
    4. Flow and pressure control for 3-component gas mixtures $10k
    5. Stainless-steel gas regulators $3k
    6. Replacement laser head for PRA LN103 N_2 laser $1k
    7. x-y translation stage, 1-μm resolution $1k
    8. Trace oxygen Monitor $4k
    9. Trace H_2O Monitor $4k
    10. Fast photodiode (200 psec) $2k
    11. High-voltage power supplies (6 channels of Bertan 377) $6k
    12. Low-voltage power supplies $2k
    13. NIM electronics: crate, hex discri, quad coincidence, gate generator, counter/timer, TAC, NIM-ECL converter $10k
    14. PC-clone computer, CAMAC crate and interface $10k
    15. 192-Channel CAMAC TDC system (LeCroy 4298, 4299, and six 4291B) .. $23kh
    16. 8-channel CAMAC ADC (Lecroy 2249A) $3k
    17. Mold for plastic high-voltage feedthroughs $12k
    18. Programmable pulse generator (Tek PG2012) $10k
    19. Digital oscilloscope (Tek TDS540) $12k

Total Permanent Equipment $121k

2. Materials, Supplies, and Travel

    1. Metallization of cathode foils, winding of straw tubes $10k
    2. Components for straw-tube end plugs $10k
    3. Fixtures for straw-tube assembly $3k
    4. Stainless-steel fittings, tubing, valves, *etc.* $3k
    5. High-purity chamber gases (including CF_4 and DME) $4k

6. Components for 200-channel readout: resistors, capacitors, IC's, PC boards, cabling, *etc.* $20k

7. Operating funds for travel, publications, and miscellaneous supplies $10k

Total Materials, Supplies, and Travel **$50k**

Indirect Costs of 67% on Materials, Supplies, and Travel **$34k**

3. Total **$213k**

3 Personnel

J.G. Heinrich and C. Lu will work full time on R&D for SSC subsystems. K.T. McDonald will spend 90% of his research time in these projects. Graduate students W.S. Anderson, Y. Zhu, and one other to be named shortly will devote all their research effort to this project. Undergraduate student E. Dunn worked on the straw-tube R&D during the summer of 91, and will perform a senior-thesis project on extensions of this work in academic year 91-92. J.C. Armitage was on sabbatical leave from Carleton U. during FY91, but has now returned to Canada. Graduate student J. Weckel worked on the straw-tube project as a Research Assistant throughout FY91, but will be teaching in FY92. In addition, we benefit from access (at no cost to the SSC) to the technical staff of the Princeton High Energy Physics group which includes 1 mechanical engineers, 3 mechanical technicians, 1 electrical engineer, and 3 electrical technician. All salaries of the above people are supported by the DoE HEP Division, except for K.T. McDonald (academic year salary from Princeton University), and W.S. Anderson (NSF Predoctoral Fellow).

4 References

[1] C. Lu *et al.*, *Prototype Study of the Straw Tube Proportional Chamber*, Princeton U. preprint DOE/ER/3072-56 (Feb. 15, 1990).

[2] C. Lu and K.T. McDonald, *A Straw-Tube Tracking System for the SSC*, to appear in the Proceedings of the IISSC (Miami, Mar. 14-16, 1990).

[3] C. Lu and K.T. McDonald, *Drift-Chamber Timing Studies with a N_2 Laser*, Princeton U. preprint DOE/ER/3072-60 (June 10, 1990).

[4] W.S. Anderson *et al.*, *Addendum to the Progress Report and Renewal Request for R&D on Central and Forward Tracking*, Princeton U. (Sept. 4, 1990).

[5] C. Lu *et al.*, *Investigations of Single-Electron Avalanches in a Proportional Drift Tube*, Proceedings of the Symposium on Detector Research and Development for the Superconducting Super Collider, ed. by T. Dombeck, V. Kelley, and G.P. Yost (Ft. Worth, Oct. 15-18, 1990), p. 222.

[6] J.C. Armitage *et al.*, *Mechanical Concerns for Long Straw-Tube Arrays*, Proceedings of the Symposium on Detector Research and Development for the Superconducting Super Collider, ed. by T. Dombeck, V. Kelley, and G.P. Yost (Ft. Worth, Oct. 15-18, 1990), p. 253.

[7] W.S. Anderson *et al.*, *Investigations on the Timing Performance of Some Gas Mixtures with Single Photoelectrons*, Princeton U. preprint (May, 1991).

[8] W.S. Anderson *et al.*, Investigations on the Electron Attachment of Various Gas Mixtures Containing CF_4, Princeton U. preprint (June, 1991).

[9] J. Weckel *et al.*, *A Device for Quick and Reliable Measurement of Wire Tension in Straw Tubes*, Princeton U. preprint (August, 1991).

[10] J. Va'vra, *Search for the Best Timing Strategy in High Precision Drift Chambers*, Nucl. Instr. and Meth. **225**, 445 (1985).

[11] J. Byrne, *Statistics of the Electron Multiplication Process in Proportional Counters.* Proc. Roy. Soc. Edin. **66A**, 33 (1962).

[12] F.M. Newcomer *et al.*, *High-Speed Bipolar Integrated Circuits for SSC Applications*, Nucl. Instr. and Meth. **A283**, 806 (1989).

[13] W.W. Ash *et al.*, *Design, Construction, Prototype Tests and Performance of a Vertex Chamber for the MAC Detector*, Nucl. Instr. and Meth. **A261**, 399 (1987).

[14] F. Pius, *Measurement of the Longitudinal Diffusion of a Single Electron in Gas Mixtures Used in Proportional Counters*, Nucl. Instr. and Meth. **205**, 425 (1983).

[15] B. Jean-Marie *et al.*, *Systematic Measurement of Electron Drift Velocity and Study of Some Properties of Four Gas Mixtures: A-CH_4, A-C_2H_4, A-C_2H_6, A-C_3H_8*, Nucl. Instr. and Meth. **159**, 213 (1979).

[16] L.G. Christophrou *et al.*, *Fast Gas Mixtures for Gas-Filled Particle Detectors*, Nucl. Instr. and Meth. **163**, 141 (1979).

[17] J. Fischer *et al.*, *Proportional Chambers for Very High Counting Rates Based on Gas Mixtures of CF_4 with Hydrocarbons*, Nucl. Instr. and Meth. A238, 249 (1985).

[18] R. Openshaw *et al.*, *Etching of Anode Wire Deposits with CF_4/Isobutane (80/20) Avalanches*, Proceedings of the Symposium on Detector Research and Development for the Superconducting Super Collider, ed. by T. Dombeck, V. Kelley, and G.P. Yost (Ft. Worth, Oct. 15-18, 1990), p. 253.

[19] R. Henderson *et al.*, *Wire Chamber Ageing with CF_4/isobutane and Ar/Ethane mixtures*, IEEE **NS35**, 477 (1988).

[20] R. Openshaw *et al.*, *Test of Wire Chamber Ageing with CF_4/isobutane(80/20), Ar/Ethane(50/50), and Ar/Ethane/CF_4(48/48/4)*, IEEE **NS36**, 567(1989).

[21] J. Kadyk, *Wire Chamber Aging*, Nucl. Instr. and Meth. **A300**, 436 (1991).

[22] S.E. Bozin and C.C. Goodyear, *Growth of Ionization Currents in Carbon Tetrafluoride and Hexafluoroethane*. Brit. J. Appl. Phys. **Ser. 2, Vol. 1**, 327 (1968).

[23] M. Frautschi *et al.*, *The AMY Inner Tracking Chamber*, Ohio State U. preprint (Oct. 1989), submitted to Nucl. Instr. and Meth.